RICE UNIVERSITY

Wireless Downlink Schemes in a Class of Frequency Selective Channels with Uncertain Channel State Information

by

Christopher B. Steger

A Thesis Submitted
in Partial Fulfillment of the
Requirements for the Degree

MASTER OF SCIENCE

Approved, Thesis Committee:

Behnaam Aazhang , Chair
J.S. Abercrombie Professor of Electrical
and Computer Engineering

Joseph Cavallaro
Professor of Electrical and Computer
Engineering

Jorma Lilleberg
Adjunct Professor of Electrical and
Computer Engineering

Houston, Texas

May, 2004

ABSTRACT

Wireless Downlink Schemes in a Class of Frequency Selective Channels with Uncertain Channel State Information

by

Christopher B. Steger

The fourth generation of cellular wireless technology will be called upon to perform at data rates far exceeding those of any existing system. The most fundamental decision in the design of the physical layer of 4G wireless systems is the choice of downlink channel allocation scheme. The four prospective technologies are OFDM, TDMA, MC-CDMA, and DS-CDMA. We contend that spectral efficiency is an essential metric with which to compare the performance of the different schemes. In this thesis, we contribute in three essential areas to the analysis of broadcast spectral efficiency by accounting for the cost of channel estimation, the uncertainty of channel estimates, and the effects of a variety of frequency-selective channels. We begin by analyzing two path channels. Then we extend our analytical results to create a more versatile and practical simulation technique that serves as a useful tool for making 4G design decisions.

Acknowledgments

I would like to give thanks for the invaluable contributions of my mentors, colleagues, family and friends. This work would not have been possible without their guidance, encouragement, energy, and especially their patience.

This thesis was primarily funded through a National Defense Science and Engineering Graduate (NDSEG) Fellowship awarded by the American Society for Engineering Education. I received additional support from Texas Instruments and my friends at Nokia. I am extremely grateful to all of the individuals, organizations, and corporations who gave time and money to support my research.

Contents

List of Figures

List of Tables

Chapter 1
Introduction

The relatively brief history of cellular wireless networks can be divided into three distinct technological generations. Each successive generation has brought with it a new level of performance in response to demands from both consumers and service providers for new applications, increased capacity, and reduced costs. Now, as we see the deployment of the third generation (3G) and begin the development of the fourth generation (4G) systems, it is time to reevaluate the design decisions made in previous generations in light of the demands to be placed on the future systems. This question is too large to be addressed in any single work, and it will occupy the wireless engineering community for the next decade. However, in an attempt to find a tractable point from which to begin our analysis, we begin by considering the dominant physical-layer characteristic of any cellular system, the downlink channel allocation scheme.

The wireless spectrum is essentially free of borders or barriers except for the limits imposed by governmental organizations and the physics of propagation. For that reason, it is essential for any multi-user wireless system to organize, divide, and allocate its spectrum to the users in a sensible and efficient manner. This method of resource allocation determines the performance and character of the system more than any other single factor. For that reason, we often describe wireless systems by their multiple-access scheme alone: TDMA, CDMA, etc. This is not to say that it is the only factor governing performance, but it does place an upper bound on the attainable performance of the system. Phrased another way, the downlink scheme determines the shape of the achievable rate region for all of the users in the system. Thus, as we begin our analysis of prospective next generation systems, we start with the choice of a channel sharing method.

The choice between candidate channel allocation methods is a deceptively simple one. We should choose the scheme that allows us to achieve the best possible performance. However, we have not yet the defined the sense in which one scheme can be "better" than any other. To determine the metric with which we will compare the systems, we must revisit the concept of the wireless spectrum. Physically speaking, it is an unlimited resource, but the reality of commerce and communications requires that the spectrum be divided into tightly regulated bands, each with its own designated uses and users. As a result, radio frequency (RF) bandwidth has become an extremely valuable commodity. Therefore, we must include the concept of "spectral efficiency" in our evaluation metric.

There are several valid definitions of spectral efficiency such as those in [2][4], but for purposes of this work, we will concern ourselves only with those expressed in units of bits per second per Hertz (b/s/Hz). The units of spectral efficiency represent the amount of data that a system can communicate every second divided by the bandwidth in which the system operates. Intuitively, this suggests a fundamental relationship between the concepts of mutual information, channel capacity, and spectral efficiency. In the context of communications, mutual information expresses the amount of data that can be transferred through a given channel during each use of that channel in units of bits. We arrive at spectral efficiency by scaling the mutual information according to the system bandwidth and the number of channel uses per second. The logical progression is clear, so it is from the standpoint of mutual information that we analyze spectral efficiency.

$$I(x,y) = \frac{1}{2}\log(1+SNR)(b/sym) \tag{1.1}$$

$$C^* = I(x,y)\frac{1}{T_{sym}}\frac{1}{BW}(b/s/Hz) \tag{1.2}$$

$$T_{sym} = \frac{K}{BW} \tag{1.3}$$

$$C^* = \frac{I(x,y)}{K} \tag{1.4}$$

Limits on mutual information can be thought of in terms of a capacity region or the range of achievable data rates for each user bounded by the channel capacity. For the rest of the work, it is important to recognize the semantic distinction between a capacity region and an achievable rate region. Capacity regions are defined by the performance of an optimal system, so the performance of any suboptimal system can only define a proper subset of the capacity region known as the achievable rate region [24]. Thus, the achievable rate region of an optimal multiple-access scheme is equal to the capacity region, and the achievable rate regions of all other schemes are contained within it.

Previous works have conducted information theoretic analyses of different multiple-access schemes in terms of both ergodic and delay-limited capacities for a number of fading conditions [24][25][14][15]. In those works, the achievable rate regions of both optimal and suboptimal systems were studied under the assumption that perfect knowledge of the channel fading condition was available to both the transmitter and the receiver. Thus, the transmitter was able to implement optimal power control, and the receiver performed optimal multi-user detection.

In practical systems, the channel state is not known a priori and must be estimated. Channel estimation carries with it some inherent statistical imperfection due to the random nature of the channel. In addition, channel estimation requires that some system resources be reallocated from data transmission to channel probing. As explained in Chapter 2, the uncertainty of the channel estimate is inversely proportional to the resources expended in the estimation. This applies a cost to the quality of the channel estimate, and, since the quality of the channel estimate is related to the achievable rate, the cost is related to the achievable rate as well. Therefore, the process of channel estimation involves a tradeoff between sacrificing resources that could be used for data and estimating the channel well enough to effectively receive the data. The overall effects of cost and uncertainty in channel estimation on the performance of downlink schemes are the focus of this work.

Studies of the effects of channel estimation cost and uncertainty on a single-user system have been performed in [20] and [18]. In [23] the effect of channel estimation error is applied to the uplink of a multi-user code division system with multi-user detection. Those contributions and other previous work will be explored in detail in Chapter 2. In this work, we use similar techniques to calculate the achievable rate regions of several downlink schemes with channel estimation, and we observe the impact of both the associated cost and uncertainty when the results are contrasted with those in [24] [25] [14] [15]. Hence, we are able to reevaluate the spectral efficiency of the various schemes under more realistic assumptions.

In addition to the introduction of uncertain channel state information (CSI) into the dominant downlink schemes, we analyze our systems in a class of rudimentary frequency-selective channels. The idea of mutual information subject to uncertain CSI in vector channels is introduced in [18] and explored in a MIMO context in [20]. However, in this work we develop a new method for analyzing each of the schemes in our simple multipath channels that differs from previous work in that it considers only a single symbol at a time while incorporating the characteristics of each scheme.

Explicitly, whereas other methods for evaluating channels with memory require the analysis of an entire frame at a time and thus become computationally overwhelming, our method uses careful analysis of the smallest possible interval to insure that the resulting equations can be computed in a reasonable fashion.

The work is organized as follows. We begin in Chapter 2 with a review of fundamental and related works in the area in order to familiarize the reader with any unfamiliar concepts and highlight the connections and differences between this work and those that came before. Then we continue to Chapter 3 and develop our problem statement further by examining channel and system models and declaring the assumptions and definitions that we use. After thoroughly stating the problem, Chapter 4 contains our analytical results, with the most arduous calculations relegated to the appendices. Then Chapter 5 features our simulation methods and results to aid in the examination of our analytical data. We extend our simulation technique to more challenging scenarios in Chapter 6 before concluding with general observations and suggestions for future work in Chapter 7.

Chapter 2
Review of Known Results

This thesis springs in a highly organic fashion from preceding works, so is useful from both an instructional and a logical standpoint to review some previous contributions in this area. We begin by briefly tracing the fundamental roots of information theory from the inception of the field. Then we continue by reviewing the origins of multi-user information theory and its connection to the different downlink techniques with which this work is concerned. We conclude this section with an explanation of some newer works with which the reader may be less familiar. Therefore, the newer results will be treated with slightly more mathematical rigor.

2.1 Mutual Information, Capacity, and Spectral Efficiency

Mutual information is a concept that was first refined in Shannon's groundbreaking work [1]. To explain it concisely, mutual information measures the amount of information, in various units, that can be forced through a given channel by a given system in one use by the system of the channel. We will dispense with more rigorous information theoretic definitions because they are exceedingly well-understood and masterfully explained in other works such as [8]. It suffices to say that, since we are in the business of transmitting information through channels, it is only natural that mutual information should be of considerable concern.

An outgrowth of mutual information is the concept of capacity, also originated in [1]. Capacity is a specific characteristic of any communications channel, and it is expressed as the maximum mutual information that can be achieved over the particular channel. Hence, the channel capacity corresponds to the mutual information of a communications system that is optimal (though perhaps not uniquely optimal) for the given channel. However, this thesis is only minimally concerned with the behavior of optimal systems, so, while the channel capacity will serve as an upper bound to all of our results, we are content to study system performance in terms of achievable rates.

Whereas capacity is mutual information maximized over all possible systems, the achievable rate is the maximum mutual information that can be attained through proper application of a fixed system. Since the achievable rate is the maximum mutual information of the system, we can safely assume that levels of mutual information below the achievable rate are likewise attainable, though they are understandably far less desirable. Our goal in this work is to compare several fixed systems according to a fair set of criteria, so it is reasonable to use the achievable rates as metrics for our comparisons. Implicit in the use of achievable rates is the concept of spectral efficiency.

The common units of mutual information are bits per channel use, so any application to a communications system must be clarified with knowledge of the rate at which the system will use the channel. With this knowledge, we can then calculate an actual achievable data rate for the system in bits per second. However, there is still more meaning to be extracted from the data rate with knowledge of the amount of spectrum required by the system to achieve the particular rate. The measurement that captures all of these factors is spectral efficiency with units of bits per second per Hertz of bandwidth.

The study of the characteristics of spectral efficiency currently occupies many of the luminaries of the field of information theory such as Shamai, Verdu, and Caire [12], and it is indisputable that spectral efficiency is a very important measure of the performance of a communication system. It is certainly not the only way to measure system performance, but it is the way with which we will be concerned in this work. However, it is worth noting that we will not always refer to spectral efficiency explicitly. Instead, by insuring that all systems under consideration use the same bandwidth, we can guarantee that comparisons measured in achievable rate are linearly related to comparisons of spectral efficiency.

2.2 Broadcast Channels

Information theory began with the concept of a single transmitter single receiver system, but the problem became significantly more complicated with the introduction of single transmitter and multiple receiving systems. We refer to this scenario as a broadcast channel, and it is fundamental to the design and evaluation of downlink schemes like the ones considered in this thesis.

The essential problem with broadcast channels is that the transmitter wishes to pass multiple independent streams of data through multiple channels to multiple receivers. To simplify the concept, we will deal quantitatively and visually only with two receiver systems. Nonetheless, the broadcast channel is further complicated by the fact that the channels to the two receivers are not generally considered to be identical, and the transmitter may or may not have full knowledge of the different channels.

The fundamental work in the area of broadcast channel capacity was written by Cover [27] in 1972. The capacity of a single user system is limited by the power and bandwidth available to the transmitter. The same is true of the broadcast channel. Therefore it is highly intuitive that when power and bandwidth are dedicated to the transmission of one user's data that leaves less power and less bandwidth for the other user's data. Hence, there is a tradeoff between the capacities of the two users, and it is that tradeoff that defines the so-called capacity region. An example of a two user capacity region is depicted in Figure 2.1.

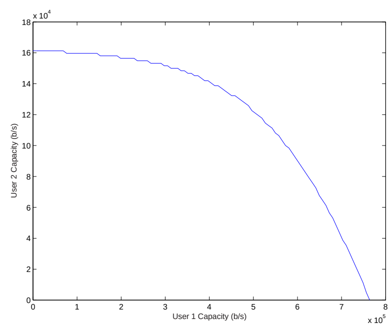

Figure 2.1 An example of a two user broadcast capacity region.

2.3 Downlink Schemes

Whereas Cover calculated the capacity region and designed an optimal broadcasting scheme, many other authors have computed similar regions for various suboptimal systems. Among the foremost researchers in the area of DS-CDMA are Shamai and Verdu [2]. Their works are generally concerned with the spectral efficiency of DS-CDMA systems with random codes in flat-fading. In addition, they often deal with large numbers of users and long spreading codes in order to capture asymptotic effects. This thesis, on the other hand, deals with a minimal number of users with minimal length orthogonal (non-random) spreading codes. Thus, the greatest connection with Verdu's work in the area of DS-CDMA is the use of spectral efficiency as the essential metric.

Other works, including those by Tse and Hanly [14] [15], and Li and Goldsmith [24] [25], feature achievable rate regions for a variety of frequency and time-division systems. Both pairs of authors were very interested in the derivation of optimal power control algorithms for use in flat-fading channels. Among the interesting results from Li and Goldsmith was the conclusion that TDMA and FDMA systems have identical achievable rate regions in flat-fading channels. As we will observe, this assumption quickly fails in the presence of frequency-selective channels. However, we should note that in this thesis we evaluate systems without the benefit of adaptive power control.

2.4 Uncertainty in Channel State Information

In all of the works mentioned previously, the authors have assumed that perfect knowledge of the channel state can be obtained by the receiver (and the transmitter as well) at no cost in terms of channel resources. Naturally, in any pragmatic system, channel state information is derived from estimation and thus contains some inherent uncertainty and error. Further, it is common practice to derive a channel estimate through the reception of a known preamble signal. Dedicating system resources to the transmission of the preamble necessarily takes away from the ability to devote those same resources to data transmission. Therefore, a balance must be struck between the need to estimate the channel and the desire to minimize preamble overhead, and the residual estimation error should be accounted for in any performance calculations.

In 2000, Medard was one of the first to deal effectively with the problem of uncertain channel state information (CSI) [18]. She derived upper and lower bounds on mutual information based on the variance of the estimation error, $\sigma^2_{\tilde{h}}$, but we will concern ourselves only with the lower bound. An expression for Medard's lower bound on a single-user system operating in a scalar channel is given in Equation 2.1.

$$I(s, y) \geq \frac{1}{2}\log(1 + \frac{h\sigma_s^2}{\sigma_n^2 + \sigma_{\tilde{h}}^2\sigma_s^2}) \tag{2.1}$$

The intuition behind Medard's result is that the worst-case scenario occurs when the channel estimation error expresses itself in the form of additional Gaussian noise.

The noise arises as a kind of self-interference due to incorrect LMMSE equalization at the receiver. Thus, the amount of additional noise is proportional to both the variance of the channel estimate and the power of the original signal.

Medard also calculated bounds for multiple user uplink systems in [18] utilizing Cover's optimal spectrum-sharing technique [26]. However, Medard's work was completely analytical and provided no actual quantitative results, and she used only ideal multi-access schemes to formulate her achievable rate regions. Thus, it serves as a valuable tool for attacking the extremely challenging problem of accounting for uncertain CSI, but it certainly does not provide all of the answers we require.

Subsequently, there have been several significant works based on Medard's example. Bhashyam, Sabharwal and Aazhang used Medard's bound to derive a feedback quantization technique and determine the effect of uncertain CSI on system performance [20]. Bhashyam, et al, worked with a multiple input multiple output (MIMO) system in a flat-fading channel, and unlike Medard, they calculated the variance of CSI uncertainty in terms of system resources devoted to channel estimation. An unrelated but likewise very important feature of [20] is the fact that the authors were faced with a very analytically and computationally complex problem. They addressed the problem by working in the smallest possible increment, in this case a single bit of feedback, and then drew inductive conclusions about the consequences of subsequent increments. Such a "baby steps" technique is extremely useful in gaining a foothold in highly complex problems, and it is used extensively in this work.

In [19] by Hassibi and Hochwald, the authors apply Medard's bound to another MIMO system with the express purpose of examining the tradeoff between channel estimation resources and system performance. Hassibi and Hochwald came to the intuitively gratifying conclusion that one should use one preamble symbol per transmit antenna. However, it is worth noting that they compromised the utility of their conclusions somewhat by failing to provide any reasonable constraints on the power allocated to the preamble symbols. As a consequence, the signal power demanded by their preamble symbols generally far exceeds that of the actual data symbols and would most likely put undue stress on power amplifier design. In this thesis, we have chosen to make the opposite assumption and conservatively limit the preamble symbols to the same power level as the data symbols. Thus, in order to improve channel estimation performance, our only degree of freedom is to change the number of preamble symbols.

Finally, Andrews and Meng produced several works focusing on the effect of uncertain CSI on a MC-CDMA uplink system in a frequency selective channel [22]. Their work focused mainly on algorithm development in the areas of power control and interference cancellation. They did not use Medard's bound and chose instead to generate channel estimation error experimentally. However, their work was notable with regard to an important assumption that we have chosen to adopt for this work as well. We assume that our receiver structures possess sufficient computational ability to iterate their nonlinear interference cancellation algorithms to the point where the only residual error comes from channel estimation error rather than detection errors. Hence, we avoid an analytical complication at the expense of the assumption of additional computational complexity. In Chapter 6, we modify this assumption by introducing some bit errors in the cancelled signal to produce more realistic results.

Chapter 3
Problem Definition

3.1 Channel Models

In examining different channel allocation techniques, we observe that they can be divided into those schemes that are defined in the frequency domain and those that are defined in the time domain. We consider OFDM and MC-CDMA to be frequency-domain systems, and we say that TDMA and DS-CDMA are time-domain systems. As result, it has become common practice to define the channels in the same domain as their corresponding systems. For flat-fading (only one resolvable path) the difference between a fading channel defined in frequency or time is inconsequential. However, when we introduce frequency-selective fading in which more than one multipath component is resolvable, significant discrepancies emerge between channels defined in the two domains. A flat-fading channel can be described with a complex scalar multiplier as seen in Equation 3.1 where input x is put through channel h and subjected to additive noise n to make output y. In this case, all of the variables are complex scalars, and, at this level of generality, we could be representing either a time-domain or frequency domain channel.

$$y = hs + n \tag{3.1}$$

Equation 3.2 represents a vector channel. That is, it represents either multiple frequency bins or multiple instants of time. In this case, x, y, and n are all complex vectors, and H is a complex matrix.

$$Y = HS + N \tag{3.2}$$

$$= \begin{pmatrix} h_{1,1} & \cdots & h_{1,m} \\ \vdots & \ddots & \vdots \\ h_{n,1} & \cdots & h_{n,m} \end{pmatrix} \begin{pmatrix} s_1 \\ \vdots \\ s_m \end{pmatrix} + \begin{pmatrix} n_1 \\ \vdots \\ n_m \end{pmatrix} \tag{3.3}$$

For reasons of intuition and analytical tractability, it is common to assume that, in the chosen domain, the individual elements of the vector channel fade according to independent random processes. Thus, particularly in information theoretic analyses, it is common to assume that the multipath components of a time-domain system fade independently. Similarly, one generally assumes that the individual frequency bins of a frequency-domain system fade independently of one another as well. By examining the Fourier transforms between the time and frequency domain channels and their correlation coefficients, we see that independent fading in the time-domain induces correlated fading in the frequency-domain and vice-versa. The coefficients are calculated in Equation 3.4.

$$\rho_{f_{1,R},f_{2,R}} = \frac{\sigma^2_{h_{1,R}} - \sigma^2_{h_{2,R}}}{\sigma^2_{h_{1,R}} + \sigma^2_{h_{2,R}}} \tag{3.4}$$

$$\rho_{f_{1,I},f_{2,I}} = \frac{\sigma^2_{h_{1,I}} - \sigma^2_{h_{2,I}}}{\sigma^2_{h_{1,I}} + \sigma^2_{h_{2,I}}} \tag{3.5}$$

$$\rho_{h_{1,R},h_{2,R}} = \frac{\sigma^2_{h_{1,R}} - \sigma^2_{h_{2,R}}}{\sigma^2_{h_{1,R}} + \sigma^2_{h_{2,R}}} \quad (3.6)$$

$$\rho_{f_{1,I},f_{2,I}} = \frac{\sigma^2_{h_{1,I}} - \sigma^2_{h_{2,I}}}{\sigma^2_{h_{1,I}} + \sigma^2_{h_{2,I}}} \quad (3.7)$$

From a physical standpoint, the differences become even clearer. Independently fading subcarriers in the frequency-domain correspond to either an infinite number of independent multipath components in the time-domain [13] or a finite number of correlated multipath components as seen above. In the case where our multipath components are defined to be IID in the time-domain, the frequency-domain equivalent also has IID subcarriers. However, while it is reasonable to assume that multipath components incident at different times are independent, it is physically highly unlikely that they will have identical distributions. As a general heuristic, the delay of a multipath component is inversely related to its power [11]. Thus, the variance of a later arriving component will generally be smaller than that of an early component. Therefore, there are almost never reasonable physical channels where one can assume that both the time-domain and frequency-domain representations consist of independently fading components. As we have demonstrated, the temptation to evaluate each system in its native domain can lead to deceptive results. The extent of the associated inaccuracy will be revealed in subsequent sections, but for now it suffices to observe that it will be very important for us to evaluate each system in channels defined in both time and frequency domains in order to maintain a "level playing field" as we make performance comparisons and value judgements.

3.2 Real Notation

For a variety of reasons that become more apparent with application, it is simpler to modify the notation of our variables such that each complex element is divided into its constituent real and imaginary components. By forming new matrices according to the method illustrated in Equation 3.8, we can then work exclusively with real numbers. Thus we refer to this alternative technique as Real Notation.

$$\begin{pmatrix} y_R \\ y_I \end{pmatrix} = \begin{pmatrix} h_R & -h_I \\ h_I & h_R \end{pmatrix} \begin{pmatrix} s_R \\ s_I \end{pmatrix} + \begin{pmatrix} n_R \\ n_I \end{pmatrix} \tag{3.8}$$

Note that the above expression is a general example, and the technique must be applied separately to each channel allocation technique in order to properly match dimensions and accurately describe the physical interactions of the scheme.

3.3 Fading Distributions

In our channel models, we allow the time and frequency bins to fade according to Ricean distributions. The Ricean distribution models a channel in which multiple paths are simultaneously incident at the receiver (not resolvable from one another), and some fraction of those paths arrive directly from the transmitter while the remainder are reflected off of some scatterers in the environment. We call the parameter describing the proportion of direct to reflected signal power the Ricean K-factor. In

Equation 3.9, we show the Ricean distribution and the K-factor calculation.

$$p(r) = \frac{r}{\sigma^2}\exp(-\frac{(r^2+A^2)}{2\sigma^2})I_0(\frac{rA}{\sigma^2}); r, A \geq 0 \tag{3.9}$$

$$A^2 = \mu_R^2 + \mu_I^2 = 2\mu^2 \tag{3.10}$$

$$\sigma^2 = \sigma_R^2 = \sigma_I^2 \tag{3.11}$$

$$K(dB) = 10\log(\frac{A^2}{2\sigma^2}) \tag{3.12}$$

In the special case where there is no direct signal component, where all of the incident signal has been reflected, the Ricean random variable decomposes into a Rayleigh random variable. Equivalently, we can say that the Rayleigh density is the same as the Ricean distribution with K-factor equal to zero (negative infinity decibels is the more common notation). Equation 3.13 gives the Rayleigh density function.

$$p(r) = \frac{r}{\sigma^2}\exp(-\frac{r^2}{2\sigma^2}); r \geq 0 \tag{3.13}$$

It is vital to note that Rayleigh and Ricean densities govern only the magnitude of the fading channel's impulse response. The phase shift imposed by the Rayleigh channel is assumed to be uniformly distribution between 0 and 2π. In our analysis, it will be extremely useful to utilize an alternative form of the Ricean random variable that is coincidentally more revealing of the physical underpinnings of the probabilistic model. By combining the effects of the Ricean distributed magnitude with those of the random phase component we arrive at a complex random variable. That random variable can be interpreted as the sum of a pair of IID complex Gaussian random variables. The K-factor of the corresponding Ricean distribution is determined by the means of the Gaussians. If the Gaussians have zero mean, then the resulting complex random variable has a Rayleigh distributed magnitude. Thus, we will be able to describe our channel by using only independent Gaussian random variables. The well-known convenient properties of the Gaussian distribution will help to simplify our analysis.

3.4 Signals and Noise

We have chosen to use complex Gaussian symbols primarily for the sake of the simplicity of their use. We do not imply that Gaussian symbols are optimal for the channels and schemes in question. In fact, we strongly suspect that they are suboptimal [18]. However, it is reasonable to assume that any more practical discrete alphabet will have performance inferior to that of the Gaussian alphabet. Therefore, the impact of slightly suboptimal signaling on conclusions drawn from this work should be negligible. We also make the standard assumption that our thermal noise follows a complex Gaussian distribution. In Chapter 6, we discard the assumption of Gaussian signaling and replace it with QPSK to get a more pragmatic system comparison.

3.5 Channel Estimation

Since we intend to use some channel state information in our systems, we assume that our channels are all block fading. That is, they fade independently from one frame to another, but during an individual frame the channel remains static. The use of block fading is obviously not entirely physically accurate, but it is a very common and useful approximation for our purposes. Following the example of [19] we have assumed that we gain channel information at the receiver from the use of preamble-based channel estimation. Thus, we incur some lost of throughput due to the dedication of some channel resources to the broadcasting of the pilot signal. We can visualize the preamble in the frame structure seen in Figure 3.1.

Observe that by devoting a fraction α of each frame to the preamble we scale our average mutual information per channel use by a factor of $(1-\alpha)$ as seen in Equation 3.14.

$$R = (1-\alpha)I(S,Y) \tag{3.14}$$

In addition, since our channel contains random additive noise, our channel estimates are expected to always contain some quantity of error. Our model of the channel with uncertain channel state information (CSI) is shown in Equation 3.15.

$$H = \hat{H} + \tilde{H} \tag{3.15}$$

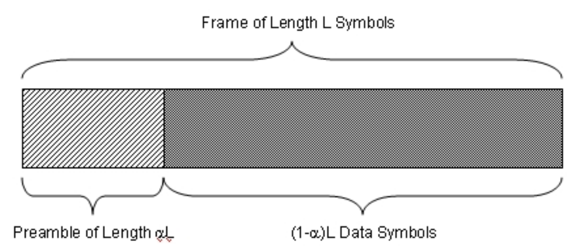

Figure 3.1 Schematic of frame containing data and preamble symbols.

$$Y = (\hat{H} + \tilde{H})S + N \tag{3.16}$$

Following the example of [18] and [20], we assume that the error in the channel estimate follows a zero-mean Gaussian distribution. In this work, we assume the use of a channel estimator that attains the Cramer-Rao Lower Bound on mean-squared estimation error of an unbiased estimator. Thus, the variance of the random variable describing the estimation error is determined according to Equation 3.17.

$$\sigma_{\tilde{h}}^2 = \frac{\sigma_n^2}{K\sigma_s^2} \tag{3.17}$$

The above expression merits a thorough inspection because it reveals the dependence of the channel uncertainty on both the number of preamble symbols (the number of separate "looks" at the channel) and the power devoted to those symbols. Whereas [19] found that it was most effective to use a minimum number of preamble symbols at power far exceeding that of the data symbols, we have chosen the somewhat more pragmatic constraint of limiting the preamble symbols to the same power level as the sum of the data symbols for both users. This prevents the transmitter's power amplifier from being faced with a "spike" at the preamble of each frame while also allowing us to reduce our experimental variables by one. However, the analysis in this work can be adapted very simply to accommodate unlimited preamble amplitude by simply adjusting the Cramer-Rao bound in Equation 3.17 and scaling the cost function (the linear factor in front of Equation 3.14) accordingly.

It is beyond the scope of this work to develop optimal training sequences. Therefore, we assume that we can achieve an upper bound on the performance of an optimal preamble. As such, we assume that each preamble symbol is received in isolation. That is, it is independent from all other preamble symbols and experiences no ISI. This is equivalent to a preamble in which all symbols remain perfectly orthogonal even after passing through the channel. We do not claim that there is any preamble sequence that can accomplish this without actually allowing an interval equal to the delay spread of the channel between preamble symbols. However, we do contend that the estimates derived from such a preamble would be at least as good as those derived from a preamble that experiences ISI.

3.6 Modelling Downlink Schemes

In this section, we define the specific downlink schemes that we will analyze. In accordance with the highly simplified channel model and the restriction to only two users, our channel sharing techniques are similarly simplified. This simplification is partly due to the fact that it facilitates analysis, but it also arises from the fact that our two path and two subcarrier channels are assumed to be viewed at the maximum resolution of the systems. Therefore, using longer spreading codes or subdividing frequency bins would contradict our channel model. These restrictions initially appear to limit the delay spreads and bandwidths of the systems in question. However, it becomes clear after further analysis that we can use our simplified systems as building blocks for systems operating in more complex channels.

3.6.1 OFDM

We make the standard assumption that each of our frequency bins experiences only flat fading, so there is no need for a cyclic prefix or other multipath mitigation. As noted earlier, OFDM is innately oriented toward a channel defined in the frequency domain. When viewed in the frequency domain, it is clear that OFDM is by definition an orthogonal spectrum sharing technique. Thus, in contrast to so-called

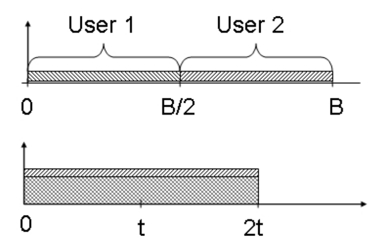

Figure 3.2 In the OFDM channel, users are orthogonal in frequency.

"superposition" systems, there is no interference between the two users and hence no need for interference cancellation. In this simple, atomic, form our OFDM system is indistinguishable from a basic FDMA system. The available bandwidth is divided equally and statically between our two users. This means that if a user is allocated no power its bandwidth remains unused. This is obviously a suboptimal design choice, but it allows for a fairer comparison with other schemes in which resource allocation is not so straightforward. In addition, giving our spectrum division the same granularity as our power allocation would give rise to either a profusion of frequency bins or a failure of our flat-fading assumptions.

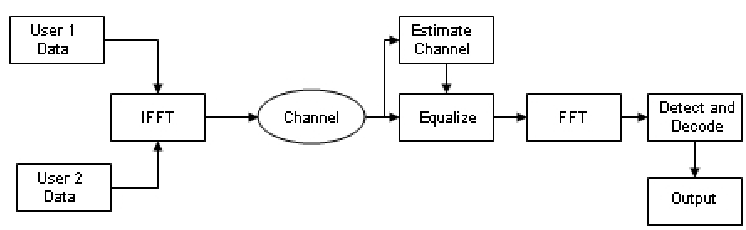

Figure 3.3 A simplified FDMA system.

3.6.2 TDMA

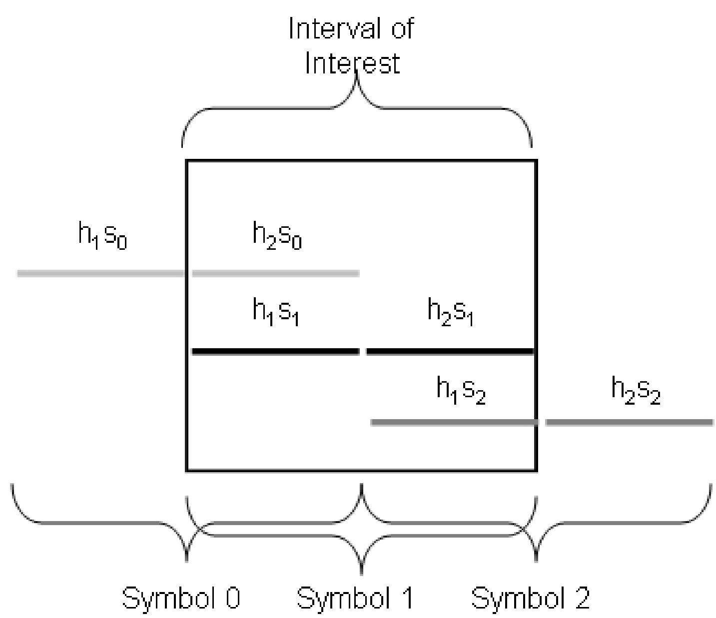

Figure 3.4 TDMA system with ISI. Note the overlapping symbols in the "interval of interest".

TDMA is our other orthogonal multiple-access technique. In a flat-fading channel, we can view it as an exact time-domain analog to our OFDM system. However, in a channel with memory, a frequency-selective channel, the analogy becomes less accurate. Whereas we can effectively ignore the effects of frequency selectivity in our OFDM system, we must provide for the mitigation of inter-symbol interference in our TDMA system. Without defining the exact algorithm, we assume the existence of a non-linear interference cancellation system. We further assume that the system uses sufficiently strong codes and sufficiently many algorithm iterations to achieve perfect knowledge of the symbols to be cancelled [23]. Therefore, the only cancellation error arises from uncertainty in the channel state information. We also assume that the interference cancellation system fully mitigates any edge effects arising from the transition from one user's time slot to the other. These assumptions are quite idealistic, so we replace them with a more practical system when we extend our results in Chapter **??**.

As in the OFDM case, we assume that if a user is allocated no power for data transmission then its time slot will remain unused. Regardless, each user is given exactly one half of each frame minus the symbols used for the shared preamble.

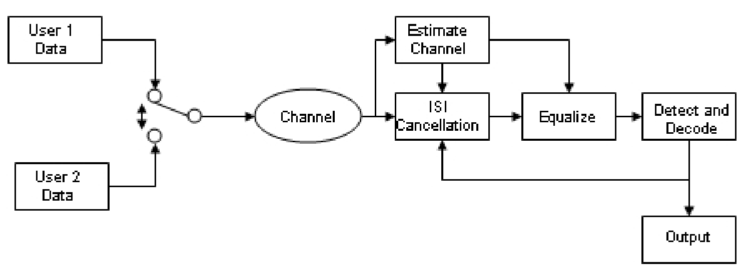

Figure 3.5 A simplified TDMA system.

3.6.3 MC-CDMA

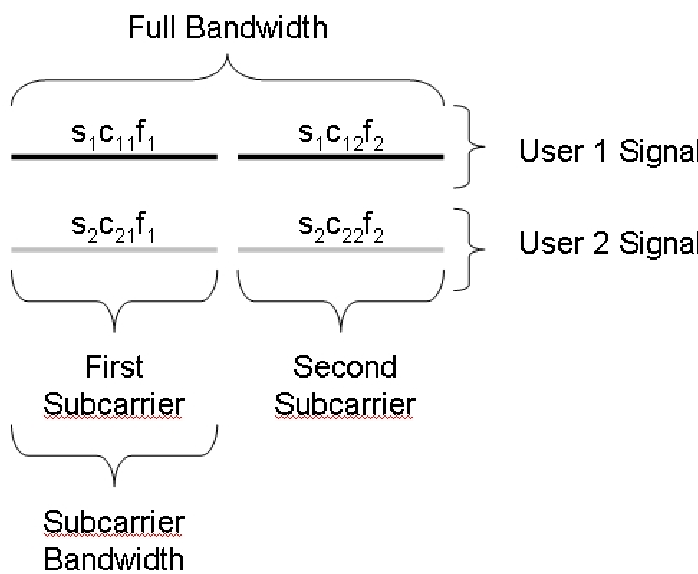

Figure 3.6 In the MC-CDMA channel, both users occupy both frequency bins simultaneously.

Our multi-carrier CDMA system uses the same frequency bins, subject to the same assumptions, as our OFDM system. However, each user has each data symbol spread over both subcarriers through the use of an orthogonal complex spreading code of length two. Hence, MC-CDMA is the first of our two superposition systems. Since there are two subcarriers and two users, spreading codes longer than two chips would be unnecessary and unfairly penalize the system. The fading of the two frequency bins may or may not be correlated, so the spreading code and its corresponding properties may be severely compromised by the channel. Thus, equalization and interference cancellation are both performed prior to despreading of the received signal. With regard to interference cancellation in MC-CDMA, we make the same basic assumptions as in TDMA. Observe that, even though we use orthogonal spreading codes, we do not rely entirely on the despreading process to remove multi-user interference. Instead, we give each user the full benefit of idealized interference cancellation subject, as always, to uncertain channel state information. In our extensions to the simulation method, we mitigate our idealized interference cancellation assumptions by accounting for bit errors remaining in the generated cancellation signal.

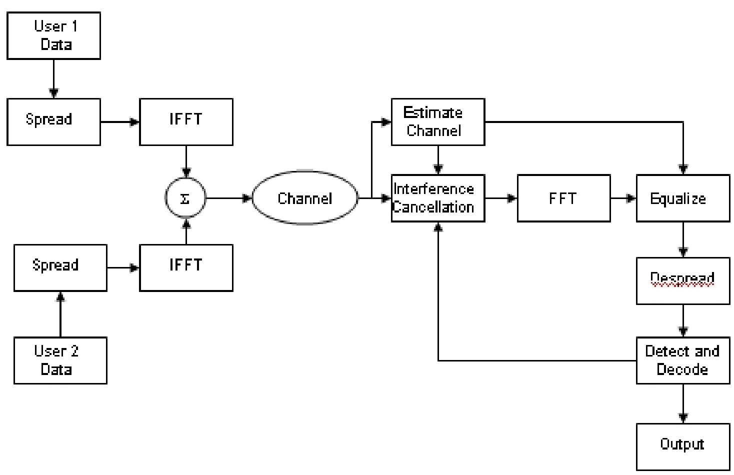

Figure 3.7 A simplified MC-CDMA channel. Note that equalization must precede despreading.

3.6.4 DS-CDMA

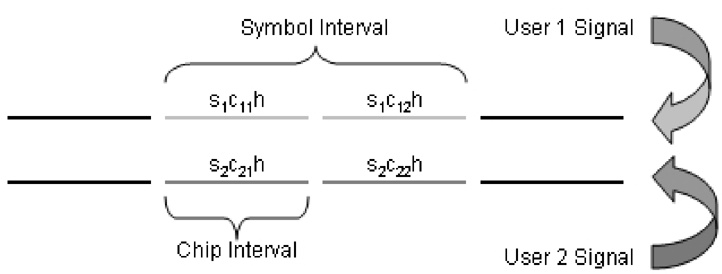

Figure 3.8 In flat fading, DS-CDMA spreading codes remain orthogonal.

As in MC-CDMA, our direct-sequence CDMA system is spread with length two complex orthogonal codes. However, the way that DS-CDMA interacts with its native channel is significantly different from MC-CDMA. Whereas MC-CDMA is spread across different frequency bins, DS-CDMA spreading codes are duplicated by the channel once per multipath component. The result is significant inter-symbol and even intra-symbol interference, but, using our assumption of exact knowledge of the path delays, the received signal can be despread prior to any equalization or interference cancellation. The spreading codes retain their properties because each pair of chips is subjected to exactly the same scalar multipath component. Of course, even after despreading, some of the same-user and multi-user interference persists and must be removed by non-linear interference cancellation. We compute our analytical results with idealized interference cancellation and then we transition to practical interference cancellation in Chapter **??**.

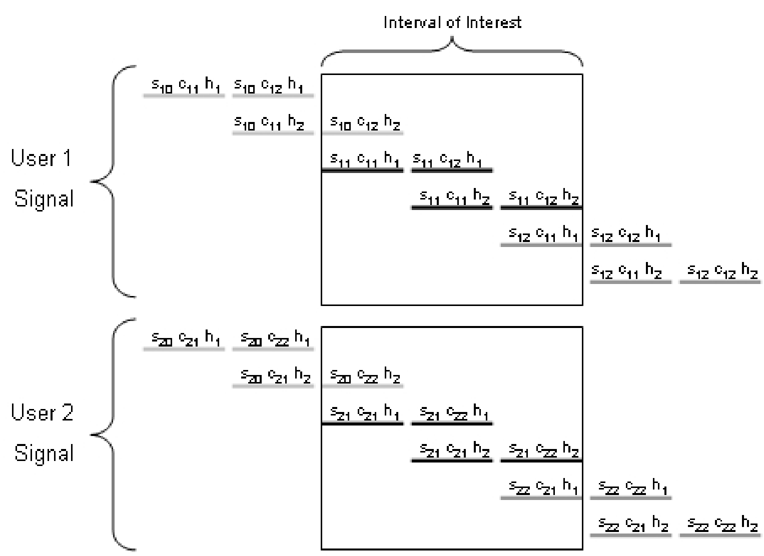

Figure 3.9 When the channel is frequency-selective, DS-CDMA users lose orthogonality and introduce ISI.

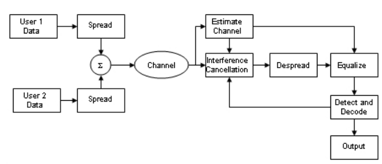

Figure 3.10 A simplified DS-CDMA system.

3.7 A Note on Signal to Noise Ratios

In works dealing with calculation of bit error rates (BER), one generally plots performance versus the signal to noise ratio (SNR). In many such cases, the SNR is a straightforward quantity. In fact, it is often an input parameter. The same is often true in works dealing with capacity and mutual information in scalar channels.

In this work, however, we deal primarily with vector (multi-bin or multipath) channels. In such channels, the concept of SNR can no longer be fully described with a single scalar parameter. Perhaps one could specify SNR per channel dimension, but interaction between channel dimensions would figure significantly into that calculation. Overall, the concept of SNR changes significantly in vector channels such that, while one can find a reasonable facsimile at the channel output, it is deceptive to try to specify it with a channel input because the value becomes highly system dependent.

Additionally, the focus of this work is to provide comparisons between different downlink schemes rather than free-standing performance numbers to be viewed in isolation. The strength of this thesis is the ability to compare different systems in the same channel. Thus, if we were to specify an SNR-like quantity at the input, it would be the same for each system in a given channel. However, the actual output SNR in the argument of each system's mutual information function is generally different, as reflected by the differing performance of each system.

Overall, any attempt to call any of our input parameters an SNR would be extremely misleading. Instead, we deemphasize the concept of SNR and look instead at individual channel parameters such as signal power, noise variance and fading variances to insure that our comparisons are reasonable and unbiased.

Chapter 4
Analysis and Analytical Results

Our analysis begins with the calculation of system and channel-specific mutual information expressions. Our methods are similar, though rather more involved, to those in [18]. Because of the complexity of the derivations, we will relegate them to the Appendices. In this chapter, we will be content to state the equations and relate the computational procedures needed to calculate their results. Explicitly, we lower bound our mutual information with the difference between the entropy of our signal and the entropy of a Gaussian random variable with the variance of our estimate.

$$I(S,Y) \geq h(S) - h(N(0, var(S - \hat{S})) \tag{4.1}$$

Reiterating that our method gives us a lower bound on actual mutual information, we state the following results.

$$\begin{aligned} I(S,Y)_{OFDM} &\geq log(\frac{\sigma s^2(\hat{f}_R^2 + \hat{f}_I^2)}{2\sigma_{\tilde{f}}^2 \sigma s^2 + \sigma_n^2} + 1) & (4.2) \\ I(S,Y)_{TDMA} &\geq \log(\frac{\sigma_s^2(h_{1,R}^2 + h_{2,R}^2 + h_{1,I}^2 + h_{2,I}^2)}{\sigma_n^2 + 4\sigma_{\tilde{h}}^2 \sigma_s^2} + 1) & (4.3) \\ I(S,Y)_{MC-CDMA} &\geq \frac{1}{2}\log(|I_4 + (\Lambda_{\tilde{F}C_1S_1} + \Lambda_{\tilde{F}C_2S_2} + \Lambda_N)^{-1}\hat{F}\Lambda_{C_1S1}\hat{F}^T|) & (4.4) \end{aligned}$$

$$I(S,Y)_{DS-CDMA} \geq \frac{1}{2}\log\left(\left|\begin{pmatrix} \Lambda_N + \Lambda_{C_1\tilde{H}C_1S_1} + \Lambda_{C_1\tilde{H}C_2S_2} \\ +\Lambda_{C_1\tilde{H}^{ISI}C_1^{ISI}S_1^{ISI}} + \Lambda_{C_1\tilde{H}^{ISI}C_2^{ISI}S_2^{ISI}} \end{pmatrix}^{-1} \hat{H}\Lambda_{S_1}\hat{H}^T + I\right|\right) \quad (4.15)$$

The notation is rather dense, but the familiar form of the mutual information expression persists in each equation. Thus, in each argument to the log, there is an SNR-like quantity consisting of a ratio of signal quantities over noise and interference quantities. Since we are dealing with matrices, the form of the ratio is not as straightforward as in the scalar case. However, we can see from the structure of each denominator that it contains all non-signal quantities. Thus, it is intuitive that we have constructed a worst-case scenario by treating all non-signal components as noise.

The form of the derivation is not so simple, though the resulting intuition is indeed quite elegant [18]. At the heart of the derivation is the use of a linear minimum mean-squared error (LMMSE) equalizer on the channel output. The estimate of the original signal has some variance related to both the variance of the noise and uncertainty about the state of the channel. It is the variance of the estimator that gives rise to the convenient form of the denominator of the SNR expression.

Once we have found our mutual information expressions in terms of the fading channels, we must then subject them to those channels in order to get an average mutual information. Even though each of our channels has only two elements, our use of real notation doubles our dimension and leads us to the quadruple integral below.

$$E_H[I(S,Y)] = \int\int\int\int I(S,Y|\hat{H})p(h_{1,R})p(h_{2,R})p(h_{1,I})p(h_{2,I})dh_{1,R}dh_{2,R}dh_{1,I}dh_{2,I} \tag{4.6}$$

In order to find the achievable rate regions pictured in this section, we compute the mutual information of each user given that each receives a certain fraction of the total available transmission power.

In calculating these results, we have several degrees of freedom. We can vary the Ricean K-factor to change the apparent proportion of direct signal to reflected signal. The choice of whether to define the statistical characteristics of the channel elements in the time domain or the frequency domain produces very different channels as well. For instance, we can modify the variances of each channel element in one domain to induce correlations in the other domain. Finally, as a benchmark, we evaluate every case with perfect CSI available at no cost to the user.

In our first scenario, Figure 4.1 we define IID Rayleigh fading on the two subcarriers with perfect CSI at the receivers. The result is identical performance from MC-CDMA and TDMA with DS-CDMA doing slightly better and OFDM doing somewhat worse.

In the second scenario, Figure 4.2, we take the same channel except we limit the users to a 1-symbol preamble. Every system suffers some performance degradation with DS-CDMA being surpassed by both TDMA and MC-CDMA in the process.

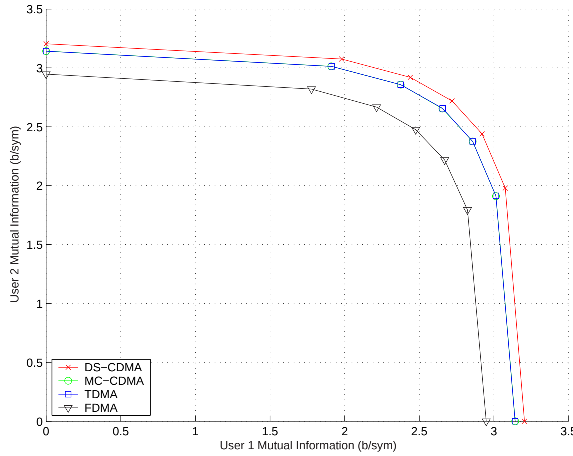

Figure 4.1 Comparison between all schemes in a Rayleigh channel defined in the frequency domain with perfect CSI and zero correlation in time domain.

In particular, we observe that MC-CDMA has separated itself above TDMA in all except the center (equal power for both users) point of the region. It is interesting to note the similar shapes shared by the two superposition schemes (DS-CDMA and MC-CDMA) and the two orthogonal schemes (OFDM and TDMA). We conclude that multi-user interference rounds out the "knee" in the superposition systems, whereas the orthogonal systems are unaffected when the other user receives additional power.

It is appropriate at this point to remind ourselves that we are examining lower bounds of unknown tightness, so these are not performance guarantees. However, they do reveal interesting trends.

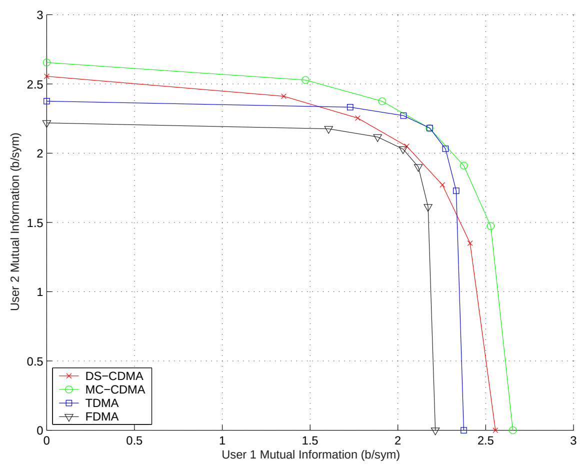

Figure 4.2 Comparison between all schemes in a Rayleigh channel defined in the frequency domain with imperfect CSI and zero correlation between multipath, analytical results.

In the next two figures, Figures 4.3 and 4.4, we repeat the process with Rayleigh channels defined in the time-domain and see very similar results. If anything, the tendencies of the frequency-domain channels seem to be further accentuated when the system is defined in time-domain.

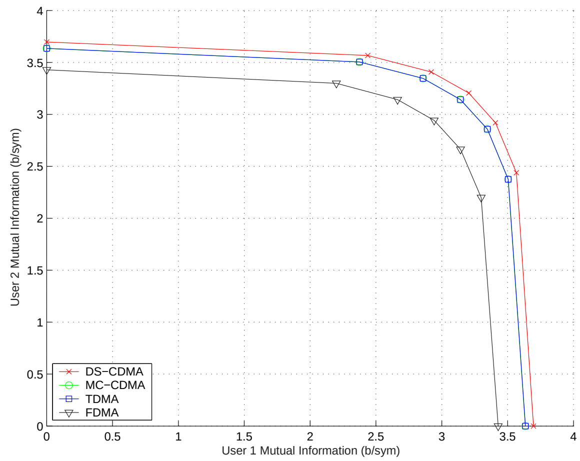

Figure 4.3 Comparison between all schemes in a Rayleigh channel defined in the time domain with perfect CSI, analytical results.

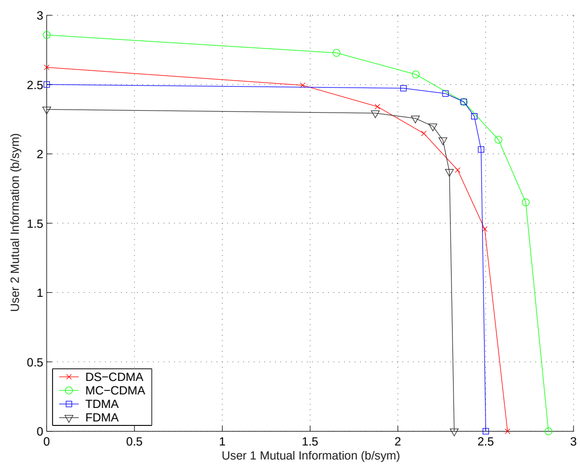

Figure 4.4 Comparison between all schemes in a Rayleigh channel defined in the time domain with imperfect CSI, analytical results.

Next we examine a frequency-domain Ricean channel with no correlation between multipath components in Figures 4.5 and 4.6.In Figure 4.5 we see that DS-CDMA holds a slight advantage with OFDM slightly worse and MC-CDMA and TDMA almost indistinguishable in the middle. However, the gap is particularly small in this example and likely to be inconsequential.

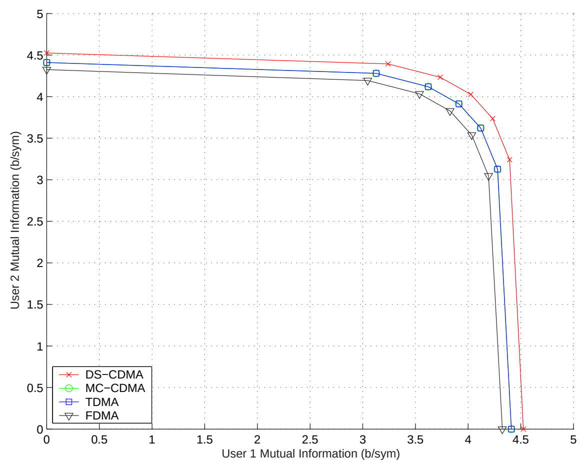

Figure 4.5 Comparison between all schemes in a Ricean channel defined in the frequency domain with perfect CSI, analytical results.

The use of a one symbol preamble degrades the performance of all schemes in Figure 4.6, as one would anticipate. It also produces the rounding effect in the MC-CDMA and DS-CDMA curves that we saw in the Rayleigh channels. Overall, the result is similar to the zero correlation Rayleigh channels.

In contrast, when we define our Ricean channel in the time domain in Figure 4.7, the typical order of performance shifts dramatically. In the perfect CSI case, DS-CDMA has become inferior with OFDM becoming the dominant system. In

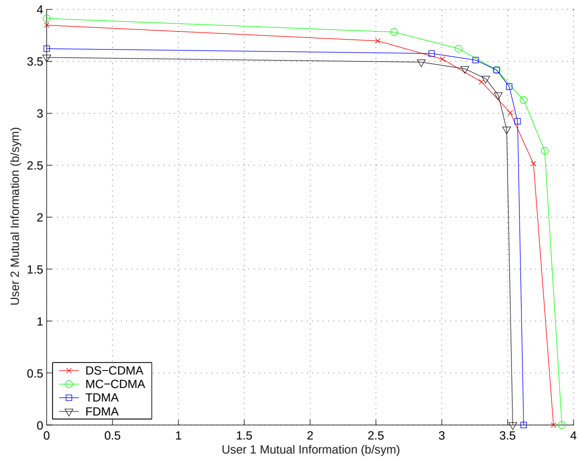

Figure 4.6 Comparison between all schemes in a Ricean channel defined in the frequency domain with imperfect CSI and no correlation in time.

this reversal we observe that the only resemblance to the Rayleigh channels and the Ricean frequency domain channels is that MC-CDMA and TDMA are once again indistinguishable.

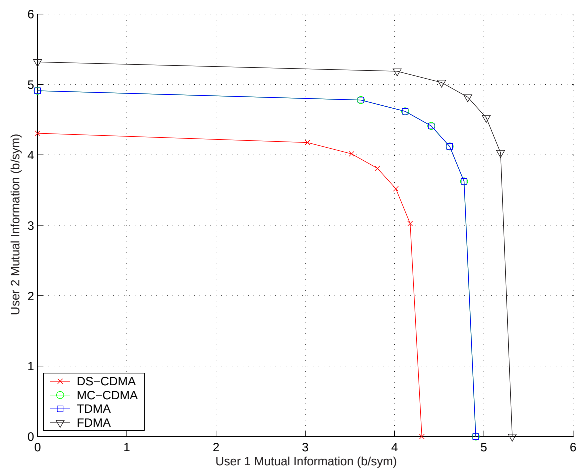

Figure 4.7 Comparison between all schemes in a Rayleigh channel defined in the time domain with perfect CSI, analytical results.

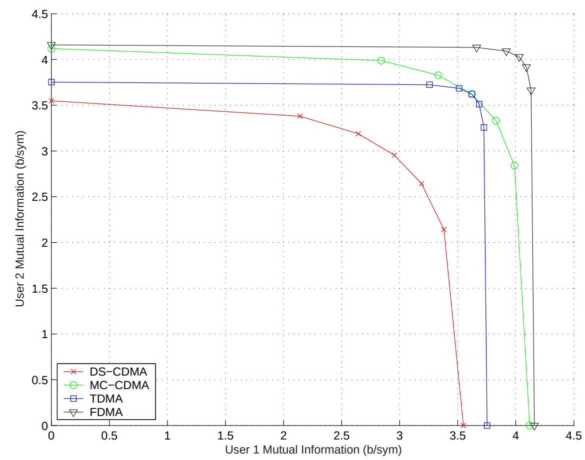

Figure 4.8 Comparison between all schemes in a Ricean channel defined in the time domain with imperfect CSI and no correlation in the time domain.

In Figure 4.8, we see the effect of degraded CSI narrows the gap between OFDM and MC-CDMA at all but the central points while DS-CDMA draws closer to TDMA but remains inferior.

In the next series of figures, we introduce channels with induced correlation between paths or subcarriers in Rayleigh fading channels. Recall that we induce correlation in one domain by unbalancing the variances of the fading variables in the other. That is, to induce correlation in the frequency domain, we make the first multipath component stronger than the second. Thus, when we induce correlation in the time domain, we create a scenario that is inherently unfair to the one of the OFDM users and overly generous to the other. It is not particularly valuable to evaluate the performance of our OFDM system in channels where we induce correlation between multipath components, but we include the results for the sake of completeness.

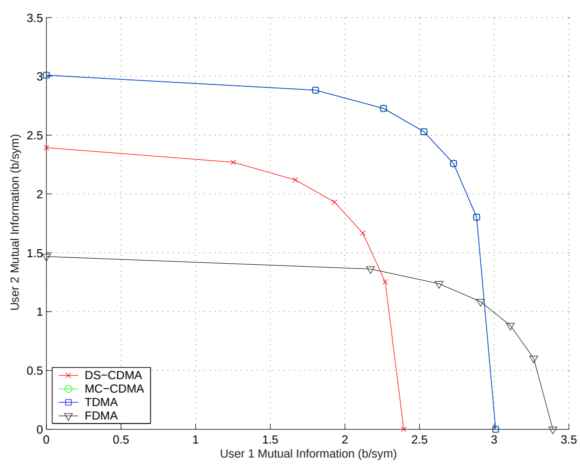

Figure 4.9 Comparison between all schemes in a Rayleigh channel defined in the frequency domain with perfect CSI and a correlation of 0.9 in the time domain, analytical results.

In Figure 4.9 we observe that the OFDM curve has indeed lost its symmetry, as expected. TDMA and MC-CDMA are again indistinguishable while DS-CDMA performs particularly poorly in this scenario. The poor performance of DS-CDMA in this scenario is difficult to rationalize intuitively since its performance was quite good in the corresponding scenario without correlation between multipath in Figure 4.1. Regardless, the discrepancy indicates the importance of careful evaluation of the assumption of IID channels.

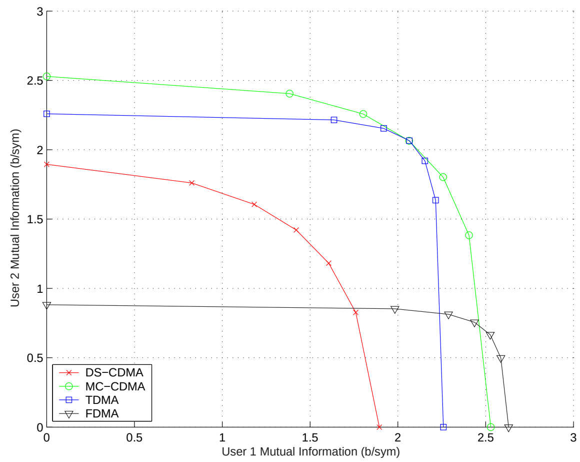

Figure 4.10 Comparison between all schemes in a Rayleigh channel defined in the frequency domain with imperfect CSI and a correlation of 0.9 in the time domain, analytical results.

Figure 4.10 shows us a Rayleigh channel with degraded CSI and a correlation of 0.9 between multipath. We see that MC-CDMA once more distinguishes itself from TDMA and becomes the dominant system in this scenario while DS-CDMA is noticeably inferior and OFDM is again distorted by our adjustment of subcarrier variances.

In contrast to the channels where we induced correlation in the time domain by adjusting frequency, in Figures 4.11 and 4.12 we see relatively little gap in performance between the different systems. In fact, the performance is very similar to

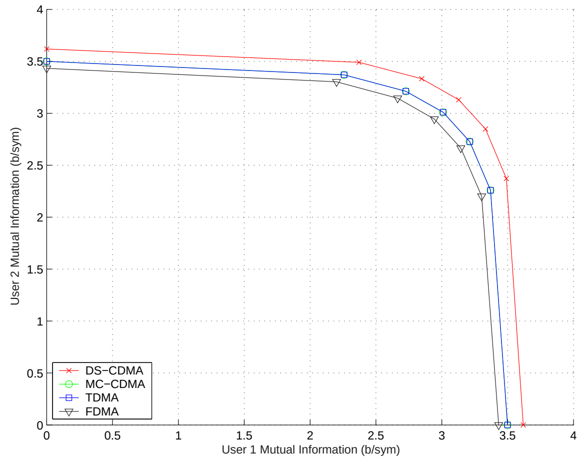

Figure 4.11 Comparison between all schemes in a Rayleigh channel defined in the time domain with perfect CSI and a correlation of 0.9 in the frequency domain, analytical results.

that seen in Rayleigh channels without correlation. Perhaps the influence would be more pronounced in OFDM or MC-CDMA systems with more subcarriers, but in our simplified case frequency domain correlation seems to have a minimal influence. We see that the perfect CSI case in Figure 4.11 favors DS-CDMA with MC-CDMA and TDMA indistinguishable and OFDM close behind.

Figure 4.12 shows the typical rounding of systems influenced by multi-access interference in degraded CSI. Once again, MC-CDMA becomes the superior system followed by TDMA, OFDM and DS-CDMA, respectively.

Overall, in this section we have seen that the relative performances of our different systems are strongly dependent on our channel definitions and assumptions about available channel state information. Thus, it is not at all fair to compare the performance of a system in a channel defined in the frequency domain with another system

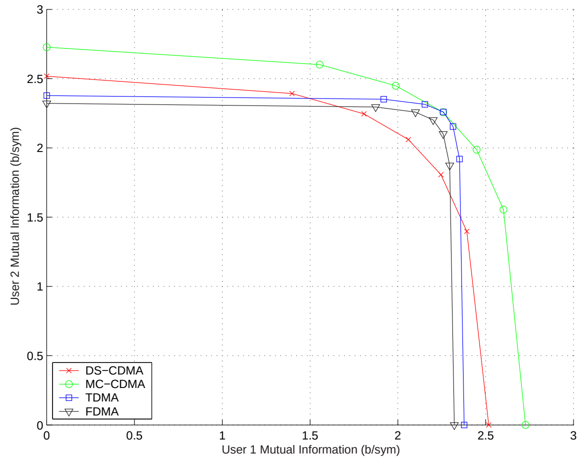

Figure 4.12 Comparison between all schemes in a Rayleigh channel defined in the time domain with imperfect CSI and a correlation of 0.9 in the frequency domain, analytical results.

in a time domain channel. In addition, correlation between multipath components has revealed itself to be an important parameter in determining performance. We still have no clear cut winner in terms of a universally superior scheme. In fact, we have seen that each system was superior at at least one point in one channel, and often the same systems were inferior in other channels. We do not have a clear answer, but we have learned much about the proper way in which to ask our questions.

Chapter 5
Simulation Methods and Results

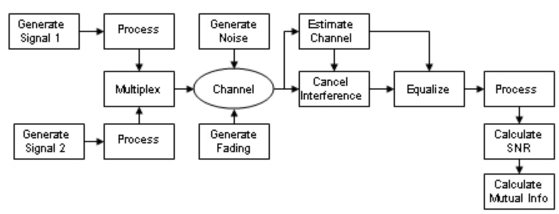

Figure 5.1 This is a schematic representation of the simulation structure.

In our simulations, we generate signals, noise, and fading according to the prescribed probability distributions. However, unlike the analytical portion of the work, we make no assumptions as to the behavior of self and multi-user interference due to uncertain CSI. In the analytical section, we calculated lower bounds by finding the worst case. In the simulation section, we verify the tightness of those bounds by not constraining the unknown signal components to be strictly noise.

We accomplish this goal by using as little a priori information as possible to separate signal and noise at the output of the channel. This complicates our task when it becomes time to calculate SNR, but we have arrived at a clever solution that has been verified by its convergence with our lower bound as the variance of our channel estimate approaches zero.

To find the magnitude of the effective signal amplitude, we project the LMMSE estimate of the signal onto the original signal. Then, to find the effective signal power, we square the magnitude of the effective signal amplitude.

In Equation 5.1, we define the effective noise amplitude as the error in the LMMSE estimate, and the effective noise power is the square of the noise amplitude. Then we simply take the ratio of effective signal power over effective noise power. This allows the interference terms to interact without constraint and contribute to either the signal or the noise terms.

$$|s_{eff}| = \frac{\langle s, \hat{s} \rangle}{|s|} \tag{5.1}$$

$$P_{s_{eff}} = |s_{eff}|^2 \tag{5.2}$$

$$n_{eff} = \hat{s} - s \tag{5.3}$$

$$P_{n_{eff}} = |n_{eff}|^2 \tag{5.4}$$

$$SNR = \frac{P_{s_{eff}}}{P_{n_{eff}}} \tag{5.5}$$

In order to find the expected mutual information, we average the mutual information over 10000 realizations of the channel, calculating SNR for each realization.

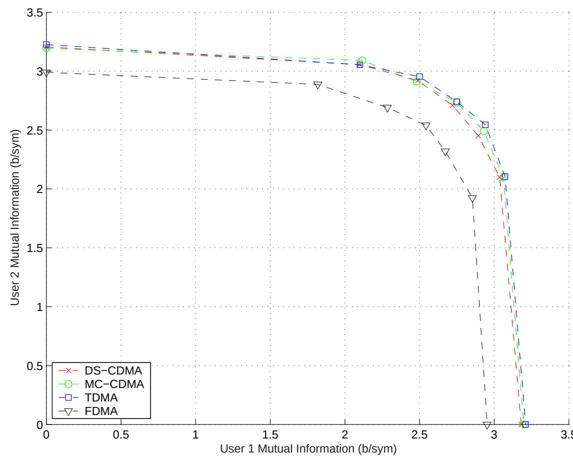

Figure 5.2 Comparison between all schemes in a Rayleigh channel defined in the frequency domain with perfect CSI, simulation results.

In Figure 5.2 we see a result similar to that which we found in Figure 4.1 in the previous chapter. In this frequency-defined Rayleigh channel with perfect CSI, DS-CDMA does not have an advantage over the other systems as it did in the analytical case. However, we do observe the same lag in performance in our FDMA system.

Figure 5.3 features a somewhat more surprising result when we introduce degraded CSI. Instead of DS-CDMA dropping down with MC-CDMA improving relative to the other systems, in this simulation DS-CDMA is slightly ahead of the other systems, which become indistinguishable from each other. This slight discrepancy between the simulation result and the analytical result in Figure 4.2 highlights the fact that, in the uncertain CSI case, our analysis calculated lower bounds, so it may not have

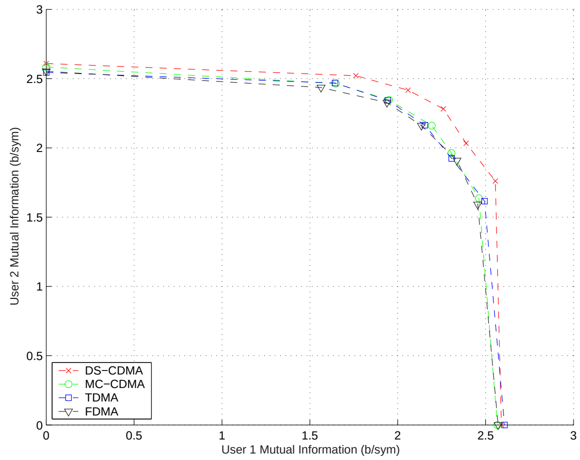

Figure 5.3 Comparison between all schemes in a Rayleigh channel defined in the frequency domain with imperfect CSI, simulation results.

captured the finer details of performance accurately. Agreement between analytical and simulation results depends significantly on the tightness of our lower bound. In the case of perfect CSI, we expect a very tight relationship between our analytical and simulated results. However, when CSI is degraded, we expect some amount of looseness to develop based on our slightly unrealistic worst-case approximation of interference as being pure AWGN.

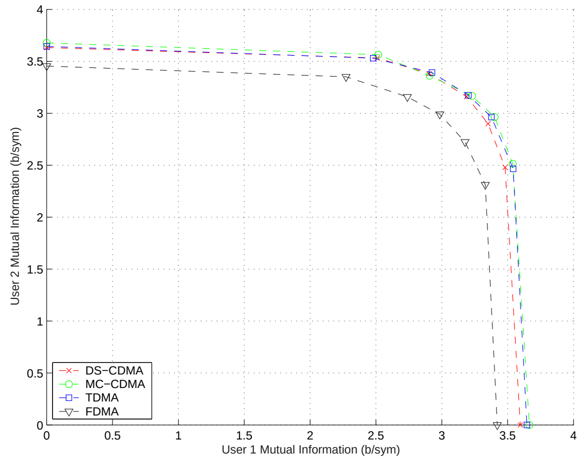

Figure 5.4 Comparison between all schemes in a Rayleigh channel defined in the time domain with perfect CSI, simulation results.

When we define our Rayleigh channel in time instead of frequency in Figure 5.4, we observe the same basic effects as in our frequency-defined channel. As expected, this is approximately identical to our analytical result in Figure 4.3.

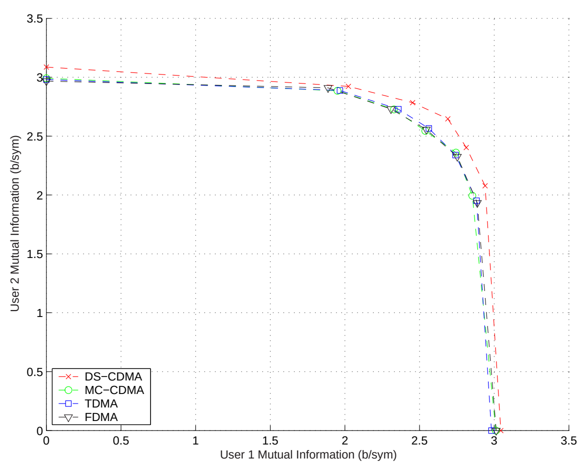

Figure 5.5 Comparison between all schemes in a Rayleigh channel defined in the time domain with imperfect CSI, simulation results.

However, Figure 5.5 shows that once again our analytical method may have missed some of the finer features of the achievable rate regions. Overall, no system distinguishes itself, though DS-CDMA does display a slight edge in the middle (equal power allocation) area. Otherwise, the systems are virtually identical.

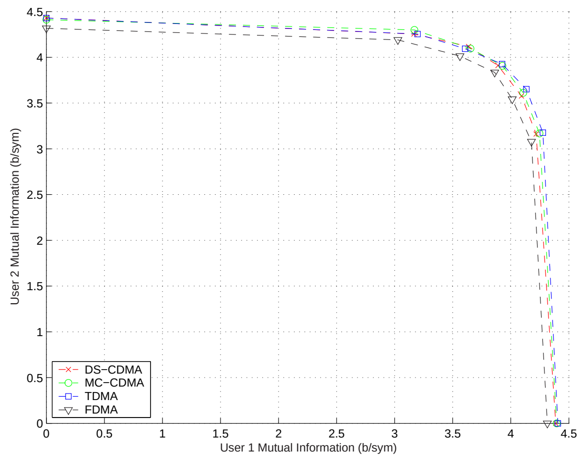

Figure 5.6 Comparison between all schemes in a Ricean channel defined in the frequency domain with perfect CSI, simulation results.

As we examine performance in a frequency-domain Ricean channel in Figure 5.6, we see very little to distinguish any system from the others. We expect this from our analytical result in Figure 4.5.

When we degrade the CSI of the Ricean channel in Figure 5.7, we still see very little performance deviation. OFDM and DS-CDMA hold a very slight advantage, but it is not notable. Again in this case, the fine features from our analytical result have failed to materialize. The apparent equality of the systems in these systems is somewhat disappointing but neither unanticipated nor unreasonable.

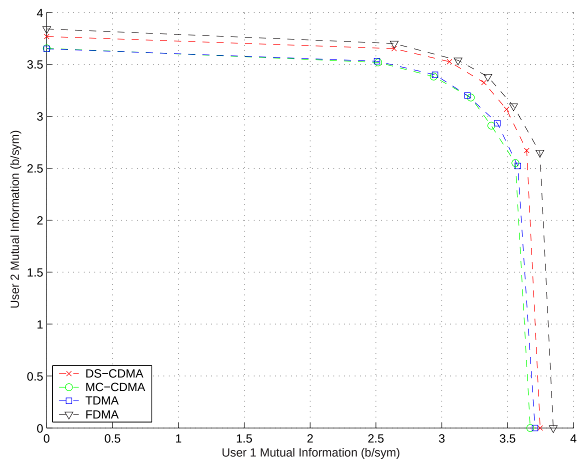

Figure 5.7 Comparison between all schemes in a Ricean channel defined in the frequency domain with imperfect CSI, simulation results.

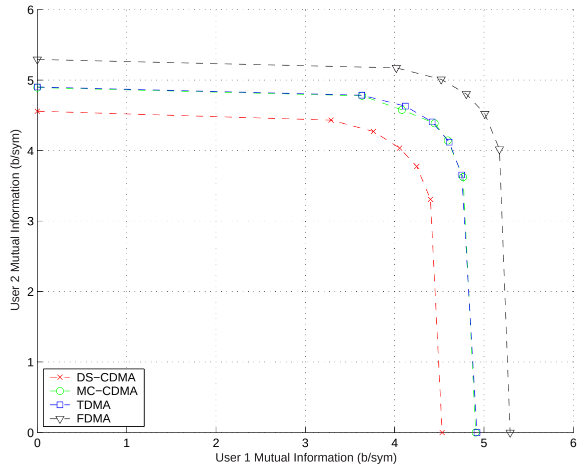

Figure 5.8 Comparison between all schemes in a Ricean channel defined in the time domain with perfect CSI and no correlation in the frequency domain.

However, before we lose hope in being able to distinguish our systems, we must examine Figure 5.8. In analytical form in Figure 4.7 we saw a relatively strong delineation between our systems. Recall that OFDM was superior with TDMA and MC-CDMA indistinguishable from each other slightly below and DS-CDMA inferior to all systems. We see these results confirmed with relatively high precision in this simulation. Clearly, more pronounced effects in our analysis can indeed carry through to our simulation results. For the first time, our simulation has produced a clearly superior system. However, recalling the ambiguity that arose in the previous chapter where each system assumed the dominant role in turn, we should withhold judgement until we see further results.

Figure 5.9 does not exactly confirm all of our observations from Figure 4.8. Most notably, we never see the achievable rate region of the MC-CDMA system differentiate

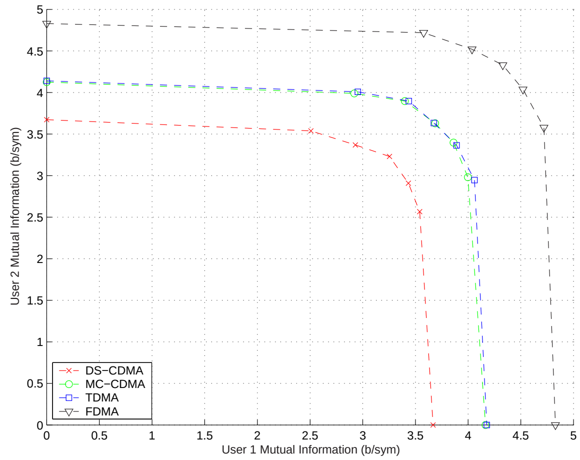

Figure 5.9 Comparison between all schemes in a Ricean channel defined in the time domain with imperfect CSI and no correlation in the frequency domain, simulation results.

itself from the TDMA region as we did in the analytical case. Nonetheless, we see the continued superiority of OFDM combined with inferior performance by DS-CDMA.

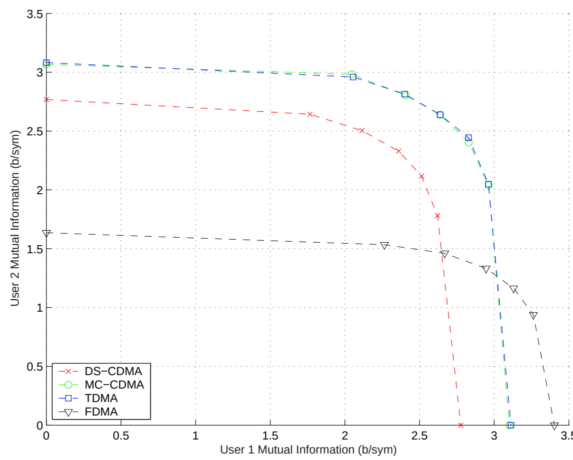

Figure 5.10 Comparison between all schemes in a Ricean channel defined in the frequency domain with perfect CSI and no correlation in the time domain, simulation results.

We introduce correlation to our multipath channel in Figure 5.10. Our analytical regions in Figure 4.9 lead us to expect dramatic results, and the simulation does not disappoint. Recalling that this channel scenario presents a distorted picture of OFDM performance, we see the same assymetrical region as in the analytical case. In addition, we observe that MC-CDMA and TDMA are indistinguishable and DS-CDMA lies significantly below, as expected.

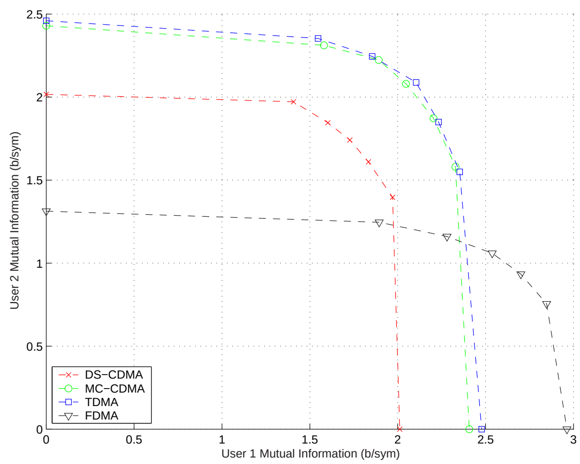

Figure 5.11 Comparison between all schemes in a Ricean channel defined in the frequency domain with imperfect CSI and no correlation in the time domain, simulation results.

As we degrade CSI in a correlated multipath channel in Figure 5.11, we see all of the features that we expected from our analytical result with the exception of MC-CDMA distinguishing itself above TDMA as the dominant system. In this case, MC-CDMA and TDMA remain equal, well above DS-CDMA.

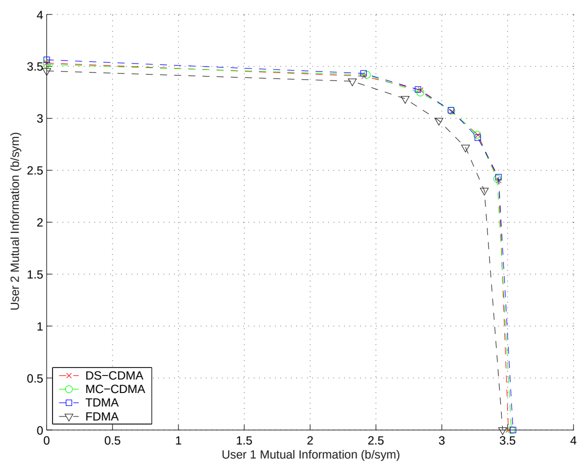

Figure 5.12 Comparison between all schemes in a Ricean channel defined in the time domain with perfect CSI and no correlation in the frequency domain, simulation results.

Our analytical results lead us to suspect that Figure 5.12 will yield little in terms of distinction between the different systems, and it fulfills that expectation. Just as in Figure 4.11 we see no remarkable features to distinguish any system. DS-CDMA tends to be equal to MC-CDMA and TDMA, while OFDM lags very slightly behind.

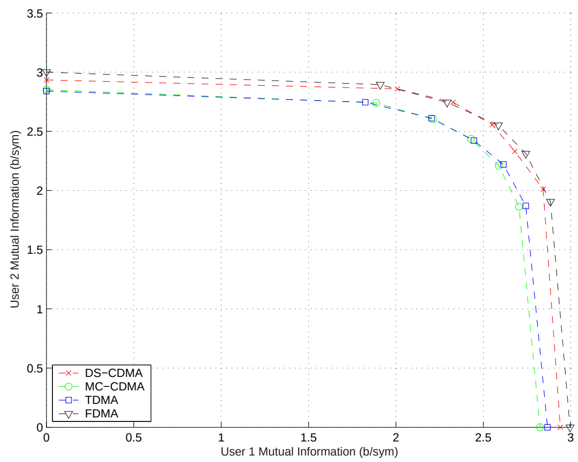

Figure 5.13 Comparison between all schemes in a Ricean channel defined in the time domain with imperfect CSI and no correlation in the time domain, simulation results.

Finally, Figure 5.13 yields a somewhat unexpected result as OFDM and DS-CDMA slightly outperform MC-CDMA and TDMA. This contradicts Figure 4.12 somewhat, though the discrepancy is within the range that we expect given our lower bound type analysis.

Overall, our simulations have muted a few of the finer features that we observed with our analytical solutions, so we have even fewer distinguishing cases than we did in the previous chapter. However, in the cases where differentiation was more pronounced, we have been able to verify our results including the curious deleterious effect of correlated multipath on DS-CDMA. Once again, we cannot declare a clear winner, but we have been able to observe some interesting cases that merit further investigation. Such cases may eventually yield a better basis for decision making, but at the very least they have shown us the importance of experimenting with a wide variety of channels rather than just making convenient assumptions.

Chapter 6
Extension of Simulation Technique to Practical Scenarios

In the previous chapter, we demonstrated a method for modelling and comparing simplified systems operating in a simplified channel. In this chapter, we adapt the simulation method to more practical, challenging scenarios. Specifically, our goals are to continue the use of mutual information and achievable rates as our metrics while abandoning some of the simplifying assumptions that facilitated our earlier simulations at the expense of applicability to realistic systems.

6.1 Simulation Methods

We continue to analyze the same four fundamental systems, OFDM, TDMA, DS-CDMA, and MC-CDMA, but we are forced to adapt them to the increasingly complicated channel conditions. However, we still retain the two user downlink paradigm, we still rely on LMMSE equalization, and we do not attempt any kind of power control at the transmitter. We have generalized our methods and system models sufficiently that they can accommodate any single input, single output (SISO) multipath channel we choose to provide, and it is reasonable to project that the methods that follow will extend easily to still more sophisticated systems.

6.1.1 Channels

Whereas we previously defined our channels in either time or frequency domain, in this chapter we restrict ourselves to channels defined in the time domain. Specifically, we focus on the four standard multipath channels used in the evaluation of 3G systems, the ITU Pedestrian A and B and Vehicular A and B channels. Using the specified parameters, we randomly generate each complex path according to a Rayleigh fading distribution. As before, we assume block fading in time.

The number of paths and their delays are specified, and we allow them to remain static. However, we assume that the systems have no a priori knowledge of the number, delays, or distributions of paths. Thus, all of the channel state information is derived, as before, from a preamble signal. We do not attempt to model mobility, so there is no Doppler shift present in our received signals.

Unlike our previous results, we specify that our systems will occupy an RF bandwidth of 20 MHz. The effects are twofold. First, we are now able to scale our mutual information results (in units of bits per channel use) to achievable rate results (in units of bits per second). The second effect arises from our ability to resolve the temporal characteristics of the channel. Our 20 MHz bandwidth is equivalent to a 10 MHz bandwidth at baseband. Therefore, we can resolve multipath components in delay bins of 50 ns [11].

6.1.2 Systems

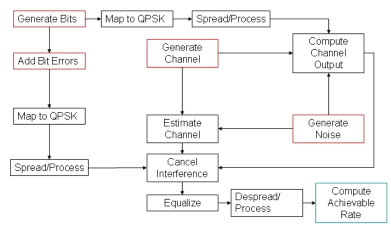

Figure 6.1 Block diagram of our simulation algorithm for realistic multipath channels.

Signaling

Mostly for reasons of analytical tractability, we previously assumed that our systems used Gaussian signaling. This assumption allowed us to simplify our mutual information expressions by setting up a simple ratio between the variances of our Gaussian signal and Gaussian noise. Unfortunately, it is not practical to implement Gaussian signaling in any realistic scheme, so in our extension we restrict ourselves to a discrete constellation. In this case, we have chosen quadrature phase shift keying (QPSK). It carries with it an inherent upper bound on mutual information since one cannot transmit more than two bits per QPSK symbol. Thus, the simulation results in this chapter upper bound the performance of the QPSK signaling subclass.

However, the technique is applicable to any finite signal alphabet.

Subcarriers

In order to retain the assumption of flat fading subcarriers, we must significantly increase the number of subcarriers used in our OFDM and MC-CDMA systems. Recall that our simplified channel model allowed us to limit ourselves to two subcarriers. This made our OFDM system indistinguishable from a basic FDMA system. We increase the number of subcarriers from 2 to 1024, so our OFDM system becomes distinct from FDMA with each user allocated 512 subcarriers.

Spreading Codes

Our original MC-CDMA system used a length 2 complex orthogonal spreading code to spread each symbol over the two subcarriers. In the interest of not over-spreading and unfairly penalizing the performance of MC-CDMA, we continue to use the length 2 spreading code. However, we must concatenate 512 codes (and hence 512 symbols) in order to spread over the full bandwidth while retaining our flat fading subcarrier assumption.

In spite of the use of length 2 spreading codes, DS-CDMA does not require a concatenation analogous to that of MC-CDMA. However, the significant complication we encounter with DS-CDMA in an ISI channel is the fact that short orthogonal spreading codes possess poor correlation properties. That is, we lose orthogonality between codes more easily than we would with longer codes. Nonetheless, we continue our use of length 2 codes to avoid unfairly penalizing DS-CDMA by spreading by a factor in excess of the number of users. It is a difficult conundrum that would resolve itself in a system with a large number of user in which we used a similarly large spreading factor. Indeed, since we are examining systems with imperfect CSI, the MC-CDMA system may experience a related performance loss due to the vulnerability of short codes to poor equalization.

In both cases, we continue to use the length 2 codes in spite of their liabilities. Whereas we could scale the results of our OFDM and TDMA simulations to larger numbers of users linearly, we note that both MC-CDMA and DS-CDMA, the superposition systems, could be expected to improve relative to the two orthogonal systems. We do not account for this scaling quantitatively, but it is important to keep it in mind when viewing the results that follow.

Interference Cancellation

The fundamental mechanics of good interference cancellation require that the interfering signal be detected and decoded as if it were the desired signal. Then the interfering signal can be recreated and convolved with the channel estimate to produce the best possible estimate for subtraction from the original received signal. In previous simulations, we assumed that there were no errors in the recreated symbols. Thus, the burden of perfection was placed on the unspecified downstream decoder, and all error in the cancellation signal was due to our uncertain knowledge of the channel.

In our more sophisticated simulations, we account for the effects of bit errors in our recreated signal. We introduce the random bit errors at a prescribed rate and then map the imperfect bit stream to the corresponding QPSK symbols. Thus, the symbol errors are not uniformly distributed. Rather, a π phase shift from correct to erroneous QPSK symbol occurs only when we have two consecutive bit errors, and a $\pm\frac{\pi}{2}$ phase shift arises from isolated bit errors. Therefore, in this chapter, we experience error in our interference cancellation arising from both residual bit errors and inaccurate channel estimates.

Note that we do not connect the bit error rate (BER) of the recreated interference signal to the SNR of that signal. Such a connection would require us to specify the downstream detectors and decoders, and such a specification is contrary to the focus of this work. Instead, our calculation of achievable rates reveals an upper bound on the performance of associated detectors and decoders.

6.1.3 Metric Calculation

In our analysis and earlier simulations, the use of Gaussian signaling proved to be a significant simplifying factor in our mutual information expressions. When we discard that assumption in favor of more realistic QPSK signaling, we are no longer able to use the mutual information expression in Equation 1.1. Instead, we must revert to the expression of mutual information in terms of the entropies of channel inputs and outputs as stated in 6.1. Where Y is the channel output and X is the channel input.

$$
\begin{aligned}
I(X,Y) &= H(Y) - H(Y|X) && (6.1)\\
H(Y) &= -\sum_{Y} p_Y(y)\log(p_Y(y)) && (6.2)\\
H(Y|X) &= -\sum_{X}\sum_{Y} p_{Y|X}(y|x)\log(p_{Y|X}(y|x)) && (6.3)
\end{aligned}
$$

Since we are using a finite signal alphabet, our input random variable is discrete. However, the presence of continuous random variables in the channel, namely Rayleigh fading and Gaussian noise, gives us a continuous output random variable. This apparently contradicts the above equations which interpret the output as a discrete random variable. We employ this discrete approximation of our continuous random variable because it arises readily from our histogram-based estimation of the probability density.

Recall that one of the principle motivations for developing this simulation method is to calculate achievable rates for signals that are received with unknown probability densities. From the entropy equations above, we see that knowledge of the density is essential to the rate calculation. Thus, we are forced to estimate the density, and we choose to do so with a histogram-based method.

Since our random variables are complex, we must construct our histograms in two dimensions. We begin by taking a vector of random variables and separating them into their real and imaginary parts. Then we find the ranges of the random variables in both dimensions. To determine the optimal histogram bin dimensions, we rely on the formula derived in [28] which is given by Equation 6.4 where W represents the bin width, N is the number of samples of the random variable, and σ is the standard deviation of the variable.

$$W = 3.49\sigma N^{-\frac{1}{3}} \tag{6.4}$$

Once we have the ranges and bin widths in both the real and imaginary dimensions, we divide the samples into two dimensional bins and count the contents of each bin. Finally, we normalize the density using the product of the number of symbols and the area (imaginary bin width multiplied by real bin width) of each bin. Thus, we have a discrete estimate of the continuous random variable, and we can use it in our entropy equations. Finally, since we have specified a bandwidth for our systems, we scale our mutual information by the bandwidth and time allocated to each user to find the achievable rate of the system.

6.2 Results and Analysis

In this section, we feature two principle types of results. First, we compare the performances of our four systems in the same manner as previous chapters. Second, we include an analysis of the effectiveness of interference cancellation with errors versus not cancelling at all. It is important to mention at this point that in all of our comparisons between systems, we use DS-CDMA and MC-CDMA with interference cancellation that suffers from a BER of 0.01. In all of these results, we have a mean received signal power 20 dB above the noise floor in the dominant (usually the first) multipath component. This is as close as we will come to a conventional notion of SNR.

6.2.1 Test Cases

We include two different test channels to verify that these simulations conform to our intuition that all of our systems should have equivalent performance in flat or non-fading channels. The first case is a non-fading AWGN channel.

No Fading

Figure 6.2 shows us that, in our simplest test case, our systems are indeed equivalent.

Figure 6.3 also meets our expectations by showing no difference in performance due to the use of interference cancellation with perfect CSI. This is intuitive because the non-fading channel does nothing to compromise the orthogonality of our spreading codes. Therefore, both the interfering signal and the erroneous signal used to try to remove it remain orthogonal to our desired signal.

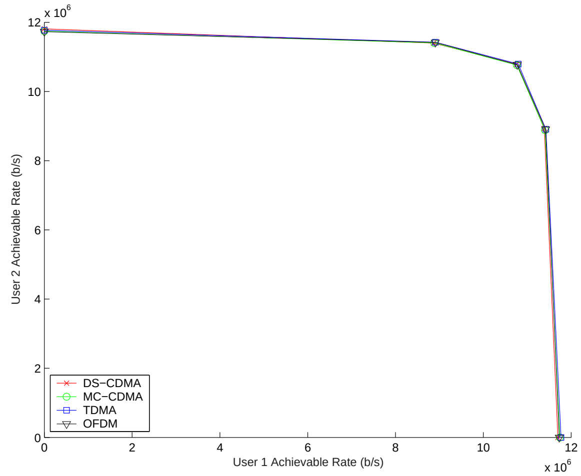

Figure 6.2 Comparison between all schemes with perfect CSI in a channel without fading, used to verify simulation methods.

Next we introduce imperfect CSI to our non-fading scenario. The intuition in this case is not as clear, but we see that the systems remain perfectly equivalent. In addition, we note that there is minimal performance degradation from the previous, perfect CSI, case, so the equalizers are evidently not challenged by this channel. Even though this channel has no fading, we continue to use the same equalizers in keeping with our assumption that the systems have no a priori knowledge of the nature of the channel.

When we examine our interference cancellation data in Figure 6.5, we again see that the equalizer has not been misled by the addition of error to the channel estimate, so interference cancellation remains irrelevant.

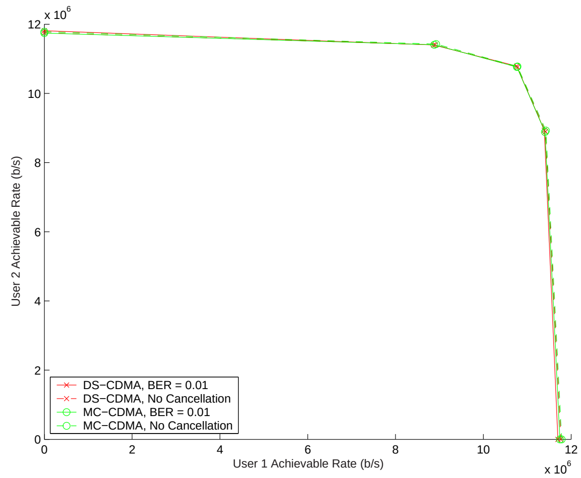

Figure 6.3 Comparison between DS-CDMA and MC-CDMA performing interference cancellation with BER of 0.01 and not cancelling at all with perfect CSI in a channel without fading, used to verify simulation methods.

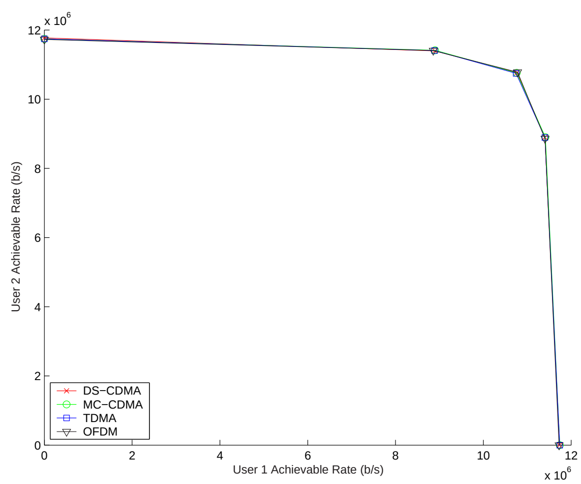

Figure 6.4 Comparison between all schemes with imperfect CSI in a channel without fading, used to verify simulation methods.

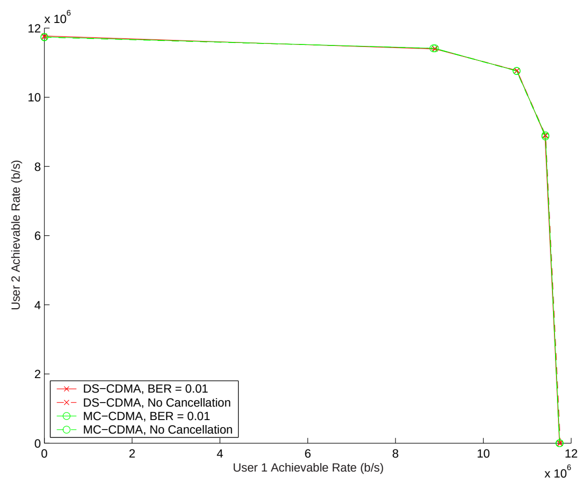

Figure 6.5 Comparison between DS-CDMA and MC-CDMA performing interference cancellation with BER of 0.01 and not cancelling at all with imperfect CSI in a channel without fading, used to verify simulation methods.

Flat Rayleigh Fading

For our next test case, we introduce flat Rayleigh fading to make sure that our systems remain approximately equivalent and to observe the effects of error in CSI. In Figures 6.6 and 6.7, we see that the achievable rates have been significantly reduced from the no fading case, but the systems remain equivalent and interference cancellation has no effect.

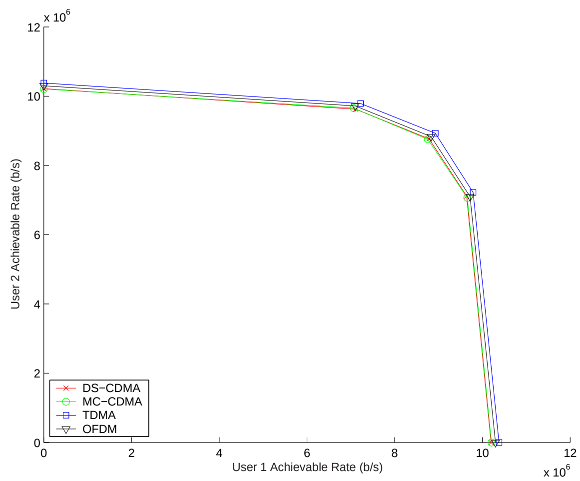

Figure 6.6 Comparison between all schemes with perfect CSI in a channel with flat Rayleigh fading, used to verify simulation methods.

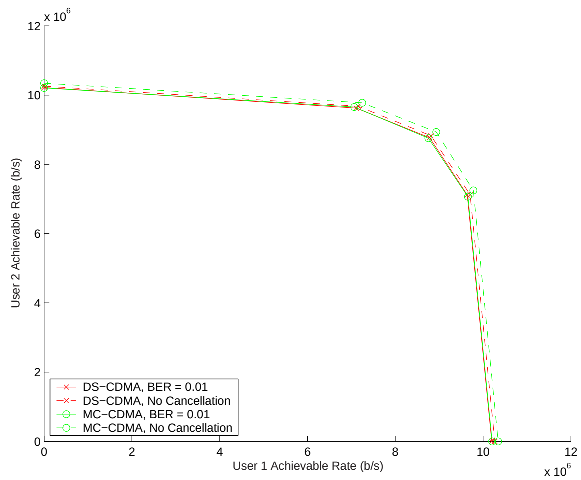

Figure 6.7 Comparison between DS-CDMA and MC-CDMA performing interference cancellation with BER of 0.01 and not cancelling at all with perfect CSI in a channel with flat Rayleigh fading, used to verify simulation methods.

When we introduce uncertain CSI in Figures 6.8 and 6.9, we begin to notice some new features. The systems begin to show a very slight separation, but it is too small for us to ascribe any significant meaning. DS-CDMA continues to show little distinction between cancelling and not cancelling interference. However, MC-CDMA shows a small advantage from not cancelling at all over cancelling with BER of 0.01.

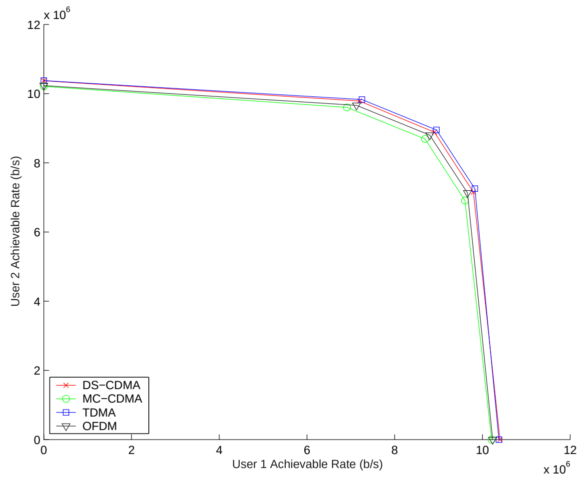

Figure 6.8 Comparison between all schemes with imperfect CSI in a channel with flat Rayleigh fading, used to verify simulation methods.

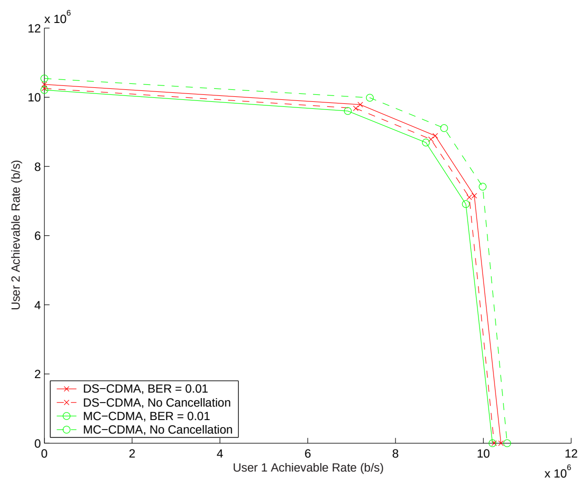

Figure 6.9 Comparison between DS-CDMA and MC-CDMA performing interference cancellation with BER of 0.01 and not cancelling at all with imperfect CSI in a channel with flat Rayleigh fading, used to verify simulation methods.

Table 6.1 Multipath parameters of the ITU Pedestrian A channel.

Tap	Relative Delay (ns)	Average Power (dB)
1	0	0
2	110	-9.7
3	190	-19.2
4	410	-22.8

6.2.2 ITU Channels

Now we have completed our test cases and we begin to examine our chosen multipath channels. We arrange the channels as follows: Pedestrian A, Pedestrian B, Vehicular A, Vehicular B.

Pedestrian A

Recall that the Pedestrian A channel has a relatively short delay spread of 410 ns and is dominated by the first multipath component. Both of these factors contribute to a relatively flat frequency response and the absence of any notable separation in the perfect CSI case in Figures 6.10 and 6.11.

However, when we introduce uncertainty to the CSI in Figures 6.12 and 6.13, we observe our first separation between systems. In this case, OFDM holds a slight

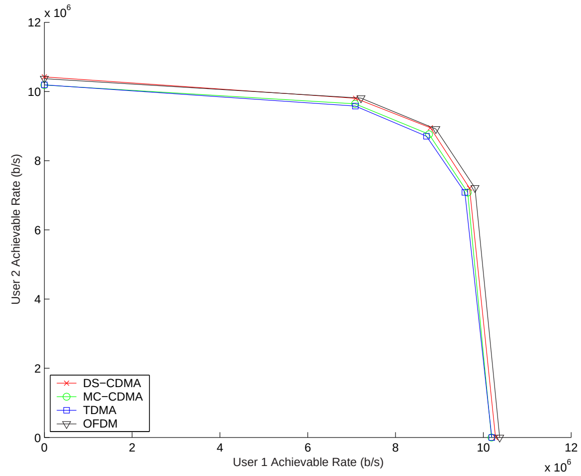

Figure 6.10 Comparison between all schemes with perfect CSI in a Pedestrian A multipath channel.

advantage over DS-CDMA and MC-CDMA with TDMA lagging behind by a small margin. With regard to interference cancellation, MC-CDMA reveals no difference, but DS-CDMA shows a small gain from using interference cancellation.

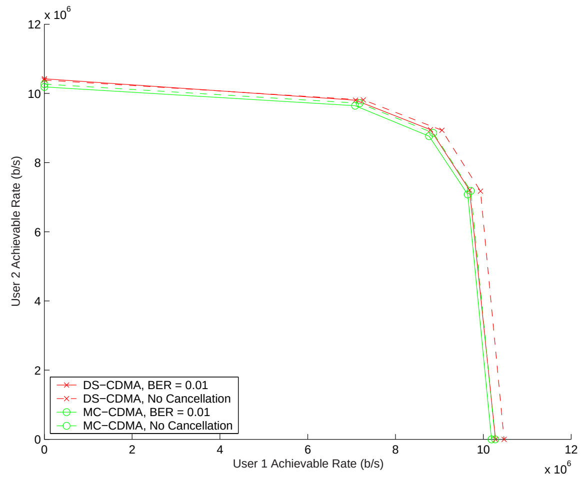

Figure 6.11 Comparison between DS-CDMA and MC-CDMA performing interference cancellation with BER of 0.01 and not cancelling at all with perfect CSI in a Pedestrian A multipath channel.

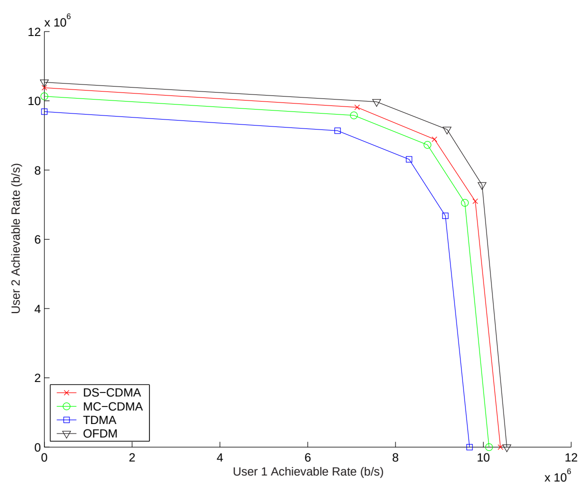

Figure 6.12 Comparison between all schemes with imperfect CSI in a Pedestrian A multipath channel.

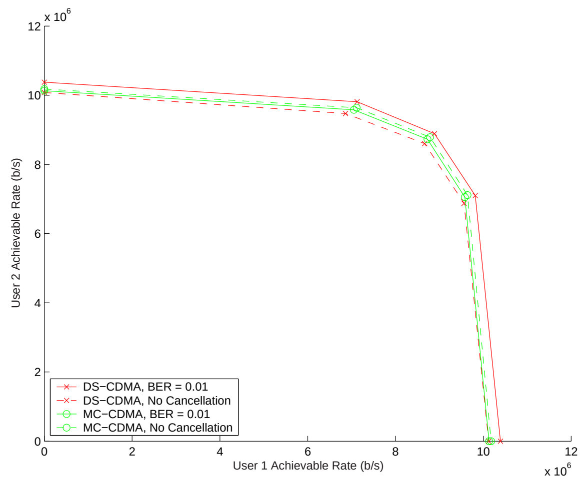

Figure 6.13 Comparison between DS-CDMA and MC-CDMA performing interference cancellation with BER of 0.01 and not cancelling at all with imperfect CSI in a Pedestrian A multipath channel.

Table 6.2 Multipath parameters of the ITU Pedestrian B channel.

Tap	Relative Delay (ns)	Average Power (dB)
1	0	0
2	200	-0.9
3	800	-4.9
4	1200	-8.0
5	2300	-7.8
6	3700	-23.9

Pedestrian B

The Pedestrian B channel poses a far greater challenge than Pedestrian A because it features 6 paths with a delay spread of 3700 ns. In addition, the first two paths are of comparable magnitude, so we expect to see deep fades in the frequency domain. In spite of this challenge, our results for the perfect CSI case show negligible impact. Thus, we conclude that our LMMSE equalizers can be quite effective when used with sufficiently long preambles.

When we shorten the preamble to a single symbol, the equalizers of all systems are obviously severely impacted and performances of all systems fall by nearly 50 percent.

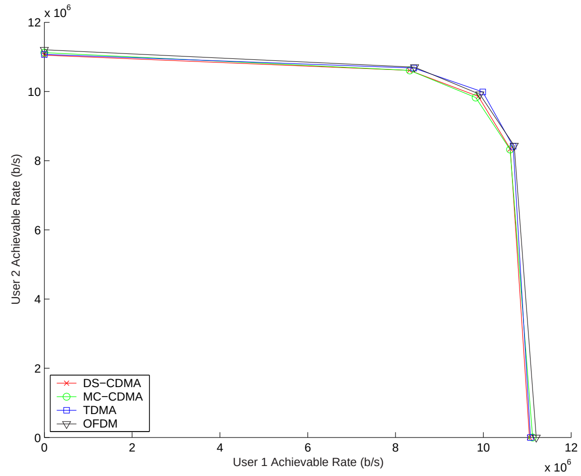

Figure 6.14 Comparison between all schemes with perfect CSI in a Pedestrian B multipath channel.

This scenario also reveals our first truly enlightening result. In Figure 6.16, we see that the OFDM system clearly dominates all others. The TDMA and DS-CDMA curves are nearly indistinguishable, and the MC-CDMA curve is slightly behind them.

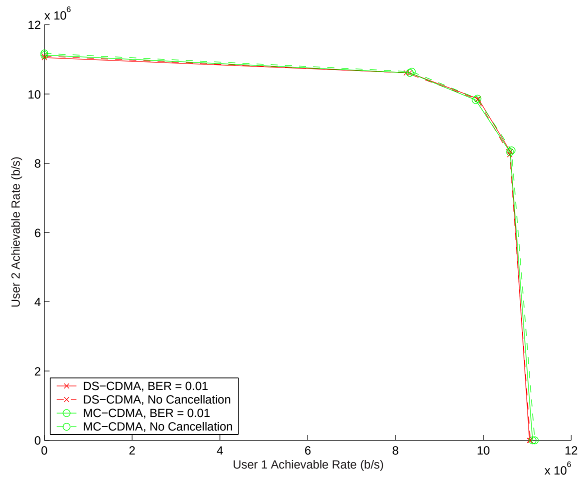

Figure 6.15 Comparison between DS-CDMA and MC-CDMA performing interference cancellation with BER of 0.01 and not cancelling at all with perfect CSI in a Pedestrian B multipath channel.

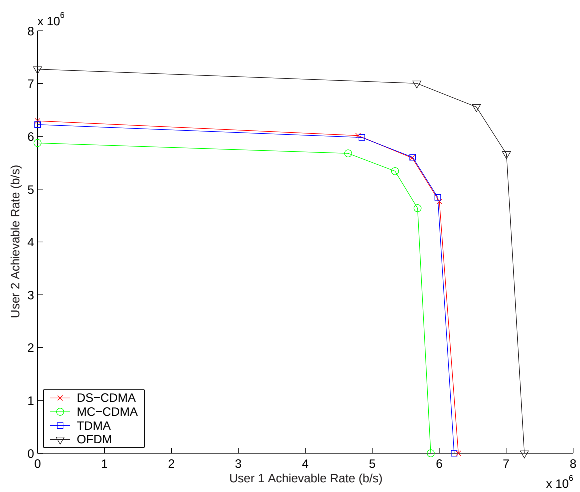

Figure 6.16 Comparison between all schemes with imperfect CSI in a Pedestrian B multipath channel.

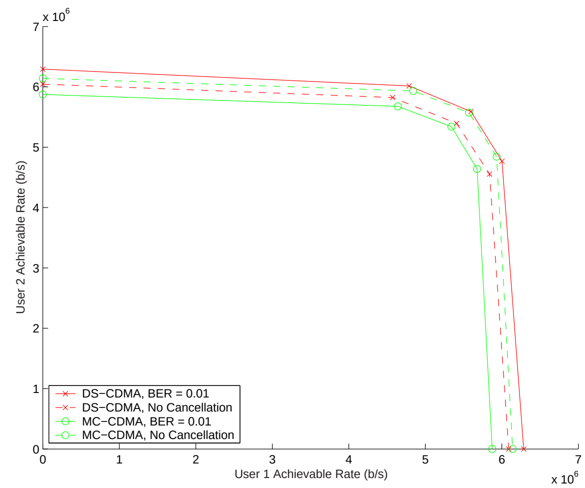

Figure 6.17 Comparison between DS-CDMA and MC-CDMA performing interference cancellation with BER of 0.01 and not cancelling at all with imperfect CSI in a Pedestrian B multipath channel.

Table 6.3 Multipath parameters of the ITU Vehicular A channel.

Tap	Relative Delay (ns)	Average Power (dB)
1	0	0
2	310	-1.0
3	710	-9.0
4	1090	-10.0
5	1730	-15.0
6	2510	-20.0

Vehicular A

The Vehicular A channel has a slightly shorter delay spread than Pedestrian B at 2510 ns, but shares the feature of two large paths with comparable magnitudes, so we expect to see it produce deep fades as well. In the pattern that has recurred throughout all of our analytical and simulation results, Figures 6.18 and 6.19 reveal little about our systems other than the effectiveness of their equalizers given perfect CSI.

In Figures 6.20 and 6.21, we begin to observe another interesting feature that figured prominently in our earlier results. We see that DS-CDMA, both with and

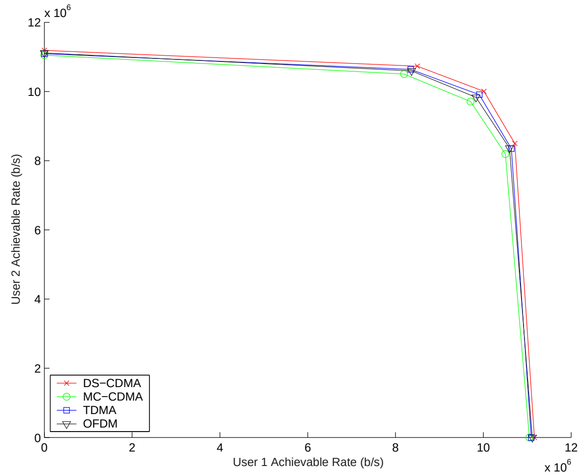

Figure 6.18 Comparison between all schemes with perfect CSI in a Vehicular A multipath channel.

without interference cancellation, takes advantage of the tails where a single user is given all of the power and outperforms all of the other systems. Then, in the middle area where power is shared equally between users, the DS-CDMA curve rounds off significantly and becomes inferior to all other systems. In addition, we observe that the degraded CSI makes it disadvantageous for either DS-CDMA or MC-CDMA to attempt interference cancellation, particularly in the equal power allocation region. In that region, no system dominates the others, but OFDM appears to hold a slight edge over TDMA. Recall that in our comparisons between systems, we use MC-CDMA and DS-CDMA with interference cancellation with BER 0.01. If we were to forsake interference cancellation altogether, both systems would be approximately comparable to TDMA and OFDM in the equal power region as seen in Figure 6.21.

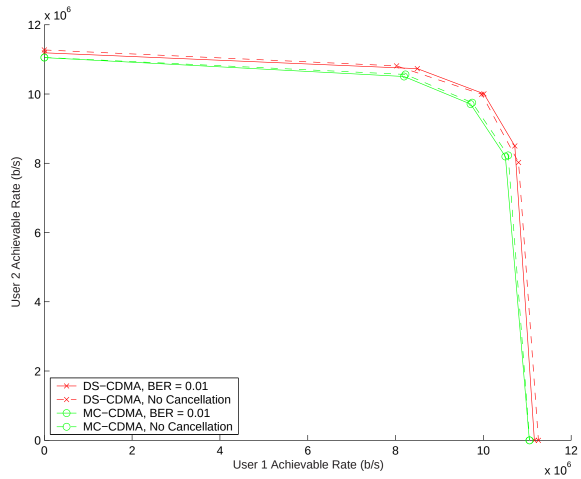

Figure 6.19 Comparison between DS-CDMA and MC-CDMA performing interference cancellation with BER of 0.01 and not cancelling at all with perfect CSI in a Vehicular A multipath channel.

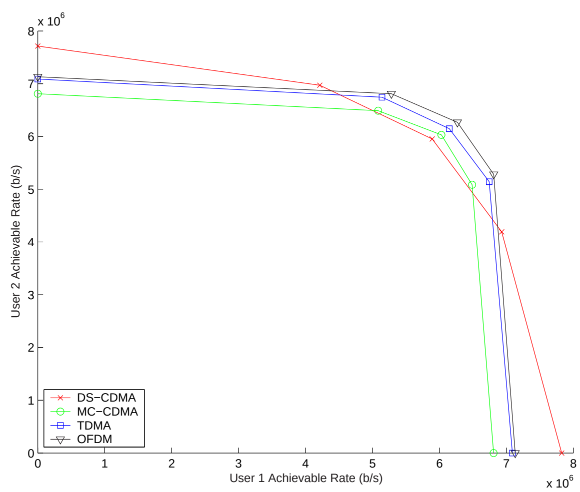

Figure 6.20 Comparison between all schemes with imperfect CSI in a Vehicular A multipath channel.

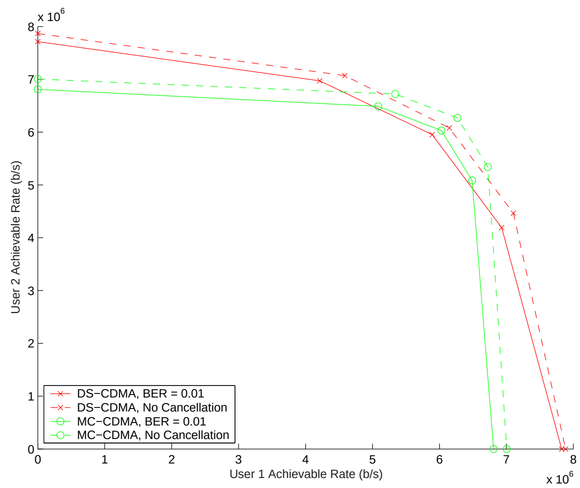

Figure 6.21 Comparison between DS-CDMA and MC-CDMA performing interference cancellation with BER of 0.01 and not cancelling at all with imperfect CSI in a Vehicular A multipath channel.

Table 6.4 Multipath parameters of the ITU Vehicular B channel.

Tap	Relative Delay (ns)	Average Power (dB)
1	0	-2.5
2	300	0
3	8900	-12.8
4	12900	-10.0
5	17100	-25.2
6	20000	-16.0

Vehicular B

The Vehicular B channel is clearly the most challenging of all. It includes two large magnitude paths and a nontrivial path arriving at a delay spread of 20 microseconds. The channel is sufficiently hostile that we even begin to see an impact in our perfect CSI case. In Figure 6.22, we see that the OFDM system is slightly inferior to the other three. It is difficult to speculate as to the exact cause of the discrepancy. However, at this point it is useful to recall that perfect channel information does not imply perfect equalization. In any equalizer, deep fades will decrease the SNR, and true nulls are completely irreversible. Thus, even though our equalizers have handled all of the previous perfect CSI cases with aplomb, we must not forget that they have limits, and apparently those limits have been exposed in the OFDM system.

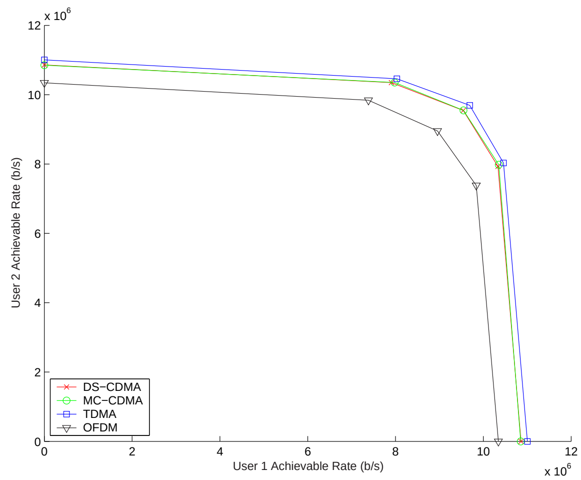

Figure 6.22 Comparison between all schemes with perfect CSI in a Vehicular B multipath channel.

Contrary to the indications from the perfect CSI case, Figure 6.24 shows us that, even though all of the systems are severely degraded by the uncertain CSI, OFDM is actually the best. On the other hand, DS-CDMA once again suffers from significant multi-user interference and falls well below the other systems in the equal power region. In fact, DS-CDMA even loses the advantage it had in the Vehicular A channel when one user dominated the other. At the tails, DS-CDMA falls behind OFDM and TDMA and is trailed only by MC-CDMA. Also worth noting is the fact that DS-CDMA derives a noticeable advantage from using interference cancellation, in spite of the 0.01 BER. Overall, every systems sees its rate reduced by more than 50 percent, but the two superposition schemes clearly suffer the most.

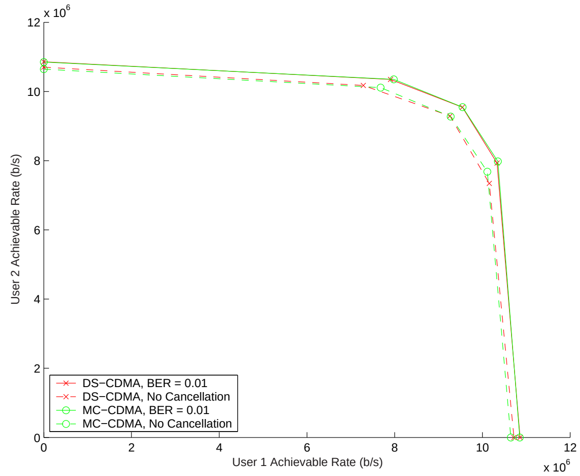

Figure 6.23 Comparison between DS-CDMA and MC-CDMA performing interference cancellation with BER of 0.01 and not cancelling at all with perfect CSI in a Vehicular B multipath channel.

When observing these results, it is important to recall the caveat from Section 6.1.2 that the short spreading codes used with DS-CDMA and MC-CDMA in our systems may not be indicative of performance with more users and longer codes.

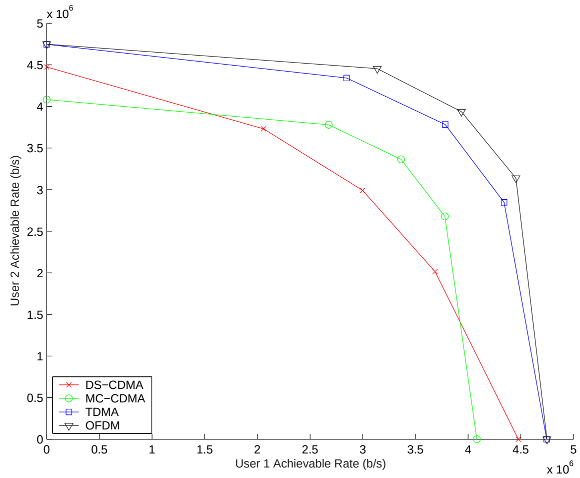

Figure 6.24 Comparison between all schemes with imperfect CSI in a Vehicular B multipath channel.

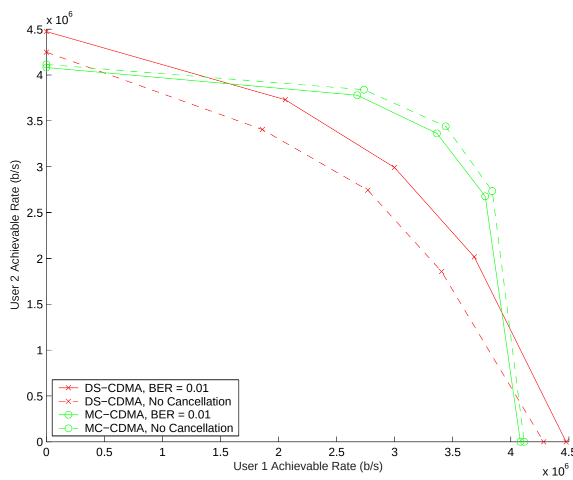

Figure 6.25 Comparison between DS-CDMA and MC-CDMA performing interference cancellation with BER of 0.01 and not cancelling at all with imperfect CSI in a Vehicular B multipath channel.

Chapter 7
Conclusions and Future Work

The most important lessons learned in this thesis are not so much conclusive answers as better formed questions. We were able to make some small differentiations between systems in different environments. For instance, MC-CDMA and TDMA appear to perform almost identically in a wide variety of scenarios while OFDM and DS-CDMA have more variable performance, sometimes surpassing and other times lagging behind. Still, we have not stated anything here that will ultimately make the decision of which downlink scheme is best for 4G.

Regardless of what that scheme turns out to be, we have demonstrated the extreme dependence on channel state information and the folly of ignoring its cost and uncertainty. Our lower bound analysis was shown to be valid, though at times the bounds were understandably loose, and our analytical and simulation methods have verified one another through their convergence in the case of good channel information.

A significant contribution of this work has been to offer a new simulation method. As one can easily see by perusing the appendices of this thesis, the possibility of expanding our analytical techniques to higher dimensional, more complicated systems is truly daunting. Not only that, but the computation of quintuple, sextuple and larger integrals would test the most impressive computing power. However, the strong performance of our simulations suggests an easier method.

Our simulations converged to theoretical values when they were supposed to do so, and they obeyed the theoretical lower bounds. Therefore, we extended them to encompass a more challenging class of channels. The computational expense of Monte Carlo type simulations is nontrivial, but it is far more tractable than the advanced numerical methods required in their analytical counterparts.

Thus, we have made some small steps toward performance comparisons rendered on a level playing field. However, the greater contribution has been the development and verification of the associated tools. We have demonstrated the strengths and shortcomings of lower-bound analysis, and we have found a more accurate, far simpler method that shows promise for future application.

Appendix A
Correlation Calculations

We observed in Chapter 3 that statistical properties of multipath components determine the correlation between the corresponding frequency bins and vice versa. In this appendix, we offer detailed calculations of those relationships.

We follow our usual convention of denoting frequency-domain coefficients by f and time-domain coefficients by h. For example, $f_{1,R}$ represents the coefficient of the real part of the first frequency bin.

$$\mu_x = E[x] \tag{A.1}$$

$$\sigma_x^2 = E[(x - \mu_x)^2] \tag{A.2}$$

$$\sigma_{xy}^2 = E[(x - \mu_x)(y - \mu_y)] \tag{A.3}$$

$$\rho_{x,y} = \frac{\sigma_{xy}^2}{(\sigma_x^2 \sigma_y^2)^{1/2}} \tag{A.4}$$

A.1 Independent Multipath, Correlated Frequency Bins

In this section, we assume that the first and second multipath components fade independently according to some Ricean distribution. That is, the real and imaginary components of each path are independent identically distributed (IID) Gaussians, and the two paths also fade independently.

$$f_{1,R} = h_{1,R} + h_{2,R} \tag{A.5}$$

$$f_{2,R} = h_{1,R} - h_{2,R} \tag{A.6}$$

$$f_{1,I} = h_{1,I} + h_{2,I} \tag{A.7}$$

$$f_{2,I} = h_{1,R} - h_{2,I} \tag{A.8}$$

Observe that the real and imaginary parts of each coefficient are independent from one another trivially.

$$\mu_{f_{(1,R)}} = E[h_{1,R} + h_{2,R}] = \mu_{h_{1,R}} + \mu_{h_{2,R}} \tag{A.9}$$

$$\mu_{f_{(2,R)}} = E[h_{1,R} - h_{2,R}] = \mu_{h_{1,R}} - \mu_{h_{2,R}} \tag{A.10}$$

$$\mu_{f_{(1,I)}} = E[h_{1,I} + h_{2,I}] = \mu_{h_{1,I}} + \mu_{h_{2,I}} \tag{A.11}$$

$$\mu_{f_{(2,I)}} = E[h_{1,I} - h_{2,I}] = \mu_{h_{1,I}} - \mu_{h_{2,I}} \tag{A.12}$$

$$\sigma^2_{f_{1,R}} = E[(f_{1,R} - \mu_{f_{1,R}})^2] \tag{A.13}$$

$$= E[f^2_{1,R}] - \mu^2_{f_{1,R}} \tag{A.14}$$

$$= E[(h_{1,R} + h_{2,R})^2] - (\mu_{h_{1,R}} + \mu_{h_{2,R}}) \tag{A.15}$$

$$= (E[h^2_{1,R}] - \mu^2_{h_{1,R}}) + (E[h^2_{2,R}] - \mu^2_{h_{2,R}}) \tag{A.16}$$

$$= \sigma^2_{h_{1,R}} + \sigma^2_{h_{2,R}} \quad (A.17)$$

$$= \sigma^2_{f_{2,R}} = \sigma^2_{h_{1,R}} + \sigma^2_{h_{2,R}} \quad (A.18)$$

$$= \sigma^2_{f_{1,I}} = \sigma^2_{h_{1,I}} + \sigma^2_{h_{2,I}} \quad (A.19)$$

$$= \sigma^2_{f_{2,I}} = \sigma^2_{h_{1,I}} + \sigma^2_{h_{2,I}} \quad (A.20)$$

Note that we have assumed that the real and imaginary components of each multipath are IID. Therefore all of the variances in Equation A.13 above are in fact equal.

$$\sigma^2_{f_{1,R}f_{2,R}} = E[(f_{1,R} - \mu_{f_{1,R}})(f_{2,R} - \mu_{f_{2,R}})] \quad (A.21)$$

$$= E[f_{1,R}f_{2,R}] - \mu_{f_{1,R}}\mu_{f_{2,R}} \quad (A.22)$$

$$\mu_{f_{1,R}}\mu_{f_{2,R}} = (\mu_{h_{1,R}} + \mu_{h_{2,R}})(\mu_{h_{1,R}} - \mu_{h_{2,R}}) \quad (A.23)$$

$$= \mu^2_{h_{1,R}} - \mu^2_{h_{2,R}} \quad (A.24)$$

$$E[f_{1,R}f_{2,R}] = E[(h_{1,R} + h_{2,R})(h_{1,R} - h_{2,R})] \quad (A.25)$$

$$= E[h^2_{1,R}] - E[h^2_{2,R}] \quad (A.26)$$

$$= (\sigma^2_{h_{1,R}} + \mu^2_{h_{1,R}}) - (\sigma^2_{h_{2,R}} + \mu^2_{h_{2,R}}) \quad (A.27)$$

$$\sigma^2_{f_{1,R}f_{2,R}} = E[f_{1,R}f_{2,R}] - \mu_{f_{1,R}}\mu_{f_{2,R}} \tag{A.28}$$

$$= ((\sigma^2_{h_{1,R}} + \mu^2_{h_{1,R}}) - (\sigma^2_{h_{2,R}} + \mu^2_{h_{2,R}})) - \mu^2_{h_{1,R}} - \mu^2_{h_{2,R}} \tag{A.29}$$

$$= \sigma^2_{h_{1,R}} - \sigma^2_{h_{2,R}} \tag{A.30}$$

$$= \sigma^2_{h_{1,I}} - \sigma^2_{h_{2,I}} \tag{A.31}$$

$$= \sigma^2_{f_{1,I}f_{2,I}} \tag{A.32}$$

$$\rho_{f_{1,R},f_{2,R}} = \frac{\sigma^2_{f_{1,R},f_{2,R}}}{(\sigma^2_{f_{1,R}}\sigma^2_{f_{2,R}})^{1/2}} \tag{A.33}$$

$$= \frac{\sigma^2_{h_{1,R}} - \sigma^2_{h_{2,R}}}{((\sigma^2_{h_{1,R}} + \sigma^2_{h_{2,R}})(\sigma^2_{h_{1,R}} + \sigma^2_{h_{2,R}}))^{1/2}} \tag{A.34}$$

$$= \frac{\sigma^2_{h_{1,R}} - \sigma^2_{h_{2,R}}}{\sigma^2_{h_{1,R}} + \sigma^2_{h_{2,R}}} \tag{A.35}$$

$$= \frac{\sigma^2_{h_{1,I}} - \sigma^2_{h_{2,I}}}{\sigma^2_{h_{1,I}} + \sigma^2_{h_{2,I}}} \tag{A.36}$$

$$= \rho_{f_{1,I},f_{2,I}} \tag{A.37}$$

Now we can see that the real parts of the two frequency coefficients are correlated as a function of the variances of the time-domain multipath components. Because of our assumption that the real and imaginary parts of each path are IID, the correlation of imaginary coefficients is the same as that of the real components.

Note that the frequency bins become uncorrelated if the multipath are IID, and they have a correlation of magnitude 1 if the variance of one multipath component goes to zero.

A.2 Independent Frequency Bins, Correlated Multipath

When we reverse our assumption and allow the frequency bins to fade independently we induce a correlation between our two multipath components in the time domain. Just as in the previous case, the real and imaginary parts of the random variables are assumed to be IID. We will forego the explicit calculation of the time-domain correlation as a function of frequency statistics since it proceeds exactly like the reverse case. Instead, we will state simply state the result.

$$\rho_{h_{1,R},h_{2,R}} = \frac{\sigma^2_{f_{1,R}} - \sigma^2_{f_{2,R}}}{\sigma^2_{f_{1,R}} + \sigma^2_{f_{2,R}}} \tag{A.38}$$

$$= \frac{\sigma^2_{f_{1,I}} - \sigma^2_{f_{2,I}}}{\sigma^2_{f_{1,I}} + \sigma^2_{f_{2,I}}} \tag{A.39}$$

$$= \rho_{h_{1,I},h_{2,I}} \tag{A.40}$$

Appendix B
Derivation of OFDM Region

In this appendix, we derive the achievable rate for only the first user since the second user's derivation would be identical. This allows us to dispense with user-specific subscripts and simplifies notation.

$$S = \begin{pmatrix} s_R \\ s_I \end{pmatrix} \tag{B.1}$$

$$F = \begin{pmatrix} f_R & -f_I \\ f_I & f_R \end{pmatrix} \tag{B.2}$$

$$N = \begin{pmatrix} n_R \\ n_I \end{pmatrix} \tag{B.3}$$

$$Y = \begin{pmatrix} y_R \\ y_I \end{pmatrix} = FS + N \tag{B.4}$$

Below we make explicit our characterization of the channel as being the sum of our channel estimate and the error in that estimate. Recall that we assume the error to be a zero-mean Gaussian random variable.

$$F = \hat{F} + \tilde{F} \tag{B.5}$$

$$E[\hat{F}|F] = F \tag{B.6}$$

$$E[\tilde{F}|F] = \begin{pmatrix} 0 & 0 \\ 0 & 0 \end{pmatrix} \tag{B.7}$$

$$E[\tilde{F}\tilde{F}^T] = \sigma_{\tilde{f}}^2 I_2 \tag{B.8}$$

Recall that our both our signal and noise are zero-mean complex Gaussian random variables as well.

$$\Lambda_S = E[SS^T] = \sigma_s^2 I_2 \tag{B.9}$$

$$\Lambda_{\tilde{F}S} = E[(\tilde{F}S)(\tilde{F}S)^T = 2\sigma_{\tilde{f}}^2 \sigma_s^2 I_2 \tag{B.10}$$

$$\Lambda_N = E[NN^T] = \sigma_n^2 I_2 \tag{B.11}$$

$$\begin{aligned}
I(S,Y) &\geq \frac{1}{2}\log(|(\Lambda_{\tilde{F}S} + \Lambda_N)^{-1}\hat{F}\Lambda_S\hat{F}^T + I_2|) && \text{(B.12)} \\
&= \frac{1}{2}\log(|(2\sigma_{\tilde{f}}^2\sigma_s^2 I_2 + \sigma_n^2 I_2)^{-1}\sigma_s^2\hat{F}\hat{F}^T + I_2|) && \text{(B.13)} \\
&= \frac{1}{2}\log(|\frac{\sigma_s^2}{2\sigma_{\tilde{f}}^2\sigma_s^2 + \sigma_n^2}\hat{F}\hat{F}^T + I_2|) && \text{(B.14)} \\
&= \frac{1}{2}\log(|\frac{\sigma_s^2}{2\sigma_{\tilde{f}}^2\sigma_s^2 + \sigma_n^2}(\hat{f}_R^2 + \hat{f}_I^2)I_2 + I_2|) && \text{(B.15)} \\
&= \frac{1}{2}\log((\frac{\sigma_s^2(\hat{f}_R^2 + \hat{f}_I^2)}{2\sigma_{\tilde{f}}^2\sigma_s^2 + \sigma_n^2} + 1)^2) && \text{(B.16)}
\end{aligned}$$

$$= \quad log(\frac{\sigma_s^2(\hat{f}_R^2 + \hat{f}_I^2)}{2\sigma_{\tilde{f}}^2\sigma_s^2 + \sigma_n^2} + 1) \tag{B.17}$$

Appendix C
Derivation of MC-CDMA Region

In the MC-CDMA case, signals are transmitted in superposition, so each user is able to "see" the other user's signal. Thus, our notation is somewhat complicated with an additional index on our signal and spreading code terms.

The indices of the spreading code reflect the user to which they belong, the index of the chip, and whether we are dealing with the real or imaginary portion of that chip. Thus $c_{1,1,R}$ is the real part of the first user's first chip.

Note that since we spread the signal over two subcarriers, our vectors and matrices will generally be twice as large as their OFDM counterparts. Hence, as our systems become more complicated, the calculation of their performance becomes likewise more challenging.

$$C_1 = \begin{pmatrix} c_{1,1,R} & -c_{1,1,I} \\ c_{1,2,R} & -c_{1,2,I} \\ c_{1,1,I} & c_{1,1,R} \\ c_{1,2,I} & c_{1,2,R} \end{pmatrix} \tag{C.1}$$

$$S_1 = \begin{pmatrix} s_{1,R} \\ s_{1,I} \end{pmatrix} \tag{C.2}$$

$$F = \begin{pmatrix} f_{1,R} & 0 & -f_{1,I} & 0 \\ 0 & f_{2,R} & 0 & -f_{2,I} \\ f_{1,I} & 0 & f_{1,R} & 0 \\ 0 & f_{2,I} & 0 & f_{2,R} \end{pmatrix} \tag{C.3}$$

$$N = \begin{pmatrix} n_{1,R} \\ n_{2,R} \\ n_{1,I} \\ n_{2,I} \end{pmatrix} \tag{C.4}$$

$$\begin{aligned} W &= FC_1S_1 + FC_2S_2 + N && \text{(C.5)} \\ &= (\hat{F} + \tilde{F})C_1S_1 + (\hat{F} + \tilde{F})C_2S_2 + N && \text{(C.6)} \end{aligned}$$

Now we include the effect of our interference cancellation by removing the second user's signal as best we can with the uncertain channel estimate.

$$\begin{aligned} W - \hat{F}C_2S_2 &= (\hat{F} + \tilde{F})C_1S_1 + (\hat{F} + \tilde{F})C_2S_2 - \hat{F}C_2S_2 + N && \text{(C.7)} \\ &= (\hat{F} + \tilde{F})C_1S_1 + \tilde{F}C_2S_2 + N && \text{(C.8)} \\ &= Y && \text{(C.9)} \end{aligned}$$

Next we formulate the LMMSE equalizer used by user 1 according to the method in [5]. Note that we are formulating the equalizer with respect to the spread signal rather than the original signal. This reflects the necessity of equalizing prior to despreading in a MC-CDMA system (see Figure 3.7).

$$\begin{aligned}
\gamma &= \Lambda_{C_1S_1,Y}\Lambda_Y^{-1} && \text{(C.10)}\\
&= \Lambda_{C_1S_1,Y}(\Lambda_{\hat{F}C_1S_1} + \Lambda_{\tilde{F}C_1S_1} + \Lambda_{\tilde{F}C_2S_2} + \Lambda_N)^{-1} && \text{(C.11)}
\end{aligned}$$

The first step makes sense because the input signal is independent of both the noise and the other user's signal, so neither has any effect on this particular matrix.

We have created the following terms for convenience. They derive their values from properties of our spreading codes.

$$\begin{aligned}
t_{1,1} &= c_{1,1,R}c_{1,2,R} + c_{1,1,I}c_{1,2,I} && \text{(C.12)}\\
t_{1,2} &= c_{1,1,R}c_{1,2,I} - c_{1,1,I}c_{1,2,R} && \text{(C.13)}
\end{aligned}$$

$$\begin{aligned}
\Lambda_{\tilde{F}C_1S_1} &= E[(\tilde{F}C_1S_1)(\tilde{F}C_1S_1)^2] && \text{(C.14)}\\
&= E\begin{pmatrix}
\frac{1}{2}(\tilde{f}_{1,R}^2 + \tilde{f}_{1,I}^2) & 0 & 0 & 0\\
0 & \frac{1}{2}(\tilde{f}_{2,R}^2 + \tilde{f}_{2,I}^2) & 0 & 0\\
0 & 0 & \frac{1}{2}(\tilde{f}_{1,R}^2 + \tilde{f}_{1,I}^2) & 0\\
0 & 0 & 0 & \frac{1}{2}(\tilde{f}_{2,R}^2 + \tilde{f}_{2,I}^2)
\end{pmatrix}\sigma_{s_1}^2 && \text{(C.15)}\\
&= \sigma_{\tilde{f}}^2\sigma_{s_1}^2 I_4 && \text{(C.16)}
\end{aligned}$$

$$
\begin{aligned}
\Lambda_{\tilde{F}C_2S_2} &= E[(\tilde{F}C_2S_2)(\tilde{F}C_2S_2)^2] && \text{(C.17)} \\
&= E\begin{pmatrix} \frac{1}{2}(\tilde{f}_{1,R}^2+\tilde{f}_{1,I}^2) & 0 & 0 & 0 \\ 0 & \frac{1}{2}(\tilde{f}_{2,R}^2+\tilde{f}_{2,I}^2) & 0 & 0 \\ 0 & 0 & \frac{1}{2}(\tilde{f}_{1,R}^2+\tilde{f}_{1,I}^2) & 0 \\ 0 & 0 & 0 & \frac{1}{2}(\tilde{f}_{2,R}^2+\tilde{f}_{2,I}^2) \end{pmatrix}\sigma_{s_2}^2 && \text{(C.18)} \\
&= \sigma_{\tilde{f}}^2\sigma_{s_2}^2 I_4 && \text{(C.19)}
\end{aligned}
$$

$$\Lambda_N = \sigma_n^2 I_4 \tag{C.20}$$

Now that we have constructed our LMMSE estimator, we use the variance of the error in the estimate of the signal to compute our mutual information. We start by defining the error.

$$E = C_1S_1 - \gamma Y \tag{C.21}$$

Then we calculate the covariance matrix of the error.

$$
\begin{aligned}
\Lambda_E &= \Lambda_{C_1S_1} - \gamma\Lambda_{Y,C_1S_1} && \text{(C.22)} \\
&= \Lambda_{C_1S_1} - \gamma\Lambda_{\hat{F}C_1S_1,C_1S_1} && \text{(C.23)} \\
&= \Lambda_{C_1S_1} - (\Lambda_{C_1S_1,Y}(\Lambda_{\hat{F}C_1S_1} + \Lambda_{\tilde{F}C_1S_1} + \Lambda_{\tilde{F}C_2S_2} + \Lambda_N)^{-1})\Lambda_{\hat{F}C_1S_1,C_1S_1} && \text{(C.24)}
\end{aligned}
$$

$$
\begin{aligned}
\Lambda_{C_1S_1} &= E[(C_1S_1)(C_1S_1)^T] && \text{(C.25)} \\
&= \begin{pmatrix} \frac{1}{2} & t_{1,1} & 0 & t_{1,2} \\ t_{1,1} & \frac{1}{2} & -t_{1,2} & 0 \\ 0 & -t_{1,2} & \frac{1}{2} & t_{1,1} \\ t_{1,2} & 0 & t_{1,1} & \frac{1}{2} \end{pmatrix} \sigma_{s_1}^2 && \text{(C.26)}
\end{aligned}
$$

$$
\Lambda_E^{-1} = \Lambda_{C_1S_1}^{-1} + \hat{F}^T(\Lambda_{\tilde{F}C_1S_1} + \Lambda_{\tilde{F}C_2S_2} + \Lambda_N)^{-1}\hat{F} \qquad \text{(C.27)}
$$

$$
\begin{aligned}
I(C_1S_1, Y) &\geq \frac{1}{2}\log(|\Lambda_{C_1S1}||\Lambda_E^{-1}|) && \text{(C.28)} \\
&= \frac{1}{2}\log(|\Lambda_{C_1S1}||\Lambda_{C_1S_1}^{-1} + \hat{F}^T(\Lambda_{\tilde{F}C_1S_1} + \Lambda_{\tilde{F}C_2S_2} + \Lambda_N)^{-1}\hat{F}|) && \text{(C.29)} \\
&= \frac{1}{2}\log(|I_4 + \hat{F}^T(\Lambda_{\tilde{F}C_1S_1} + \Lambda_{\tilde{F}C_2S_2} + \Lambda_N)^{-1}\hat{F}\Lambda_{C_1S1}|) && \text{(C.30)} \\
&= \frac{1}{2}\log(|I_4 + (\Lambda_{\tilde{F}C_1S_1} + \Lambda_{\tilde{F}C_2S_2} + \Lambda_N)^{-1}\hat{F}\Lambda_{C_1S1}\hat{F}^T|) && \text{(C.31)}
\end{aligned}
$$

Appendix D
Derivation of TDMA Region

$$H = \begin{pmatrix} h_{1,R} & -h_{1,I} \\ h_{2,R} & -h_{2,I} \\ h_{1,I} & h_{1,R} \\ h_{2,I} & h_{2,R} \end{pmatrix} \tag{D.1}$$

Note that in TDMA only one user receives at a time, so we let the index on the signal term refer to the index of the symbol rather than the user.

$$S_1 = \begin{pmatrix} s_{1,R} \\ s_{1,I} \end{pmatrix} \tag{D.2}$$

In the ISI matrix, we capture the interference caused by the symbols adjacent to the symbol of interest.

$$ISI = \begin{pmatrix} h_{2,R}s_{0,R} - h2, Is_{0,I} \\ h_{1,R}s_{2,R} - h1, Is_{2,I} \\ h_{2,R}s_{0,I} + h2, Is_{0,R} \\ h_{1,R}s_{1,I} + h1, Is_{2,R} \end{pmatrix} \tag{D.3}$$

$$W = HS + ISI + N \tag{D.4}$$

As in our other systems, we use nonlinear interference cancellation to mitigate our interference term, the ISI. Note that we preserve our convention of estimates with a hat and error in those estimates with a tilde.

$$\begin{aligned} Y &= (\hat{H}+\tilde{H})S + (\widehat{ISI} + \widetilde{ISI}) - \widehat{ISI} + N && \text{(D.5)} \\ &= (\hat{H}+\tilde{H})S + \widetilde{ISI} + N && \text{(D.6)} \end{aligned}$$

Now we derive the LMMSE estimator for the signal.

$$\begin{aligned} \gamma &= \Lambda_{S_1,Y}\Lambda_Y^{-1} && \text{(D.7)} \\ &= \Lambda_{S_1,Y}(\Lambda_{\hat{H}S_1} + \Lambda_{\tilde{H}S_1} + \Lambda_{\widetilde{ISI}} + \Lambda_N)^{-1} && \text{(D.8)} \end{aligned}$$

$$\begin{aligned} \Lambda_{\tilde{H}S_1} &= 2\sigma_{\tilde{h}}^2\sigma_s^2 I_4 && \text{(D.9)} \\ \Lambda_{S_1} &= \sigma_s^2 I_2 && \text{(D.10)} \\ \Lambda_{\widetilde{ISI}} &= 2\sigma_{\tilde{h}}^2\sigma_s^2 I_4 && \text{(D.11)} \\ \Lambda_N &= \sigma_n^2 I_4 && \text{(D.12)} \end{aligned}$$

Now that we have constructed our LMMSE estimator, we use the variance of the error in the estimate of the signal to compute our mutual information. We start by defining the error.

$$E = S_1 - \gamma Y \tag{D.13}$$

Then we calculate the covariance matrix of the error.

$$\begin{aligned}
\Lambda_E &= \Lambda_{S_1} - \gamma \Lambda_{Y,S_1} && \text{(D.14)}\\
&= \Lambda_{S_1} - \gamma \Lambda_{\hat{H}S_1,S_1} && \text{(D.15)}\\
&= \Lambda_{S_1} - (\Lambda_{S_1,Y}(\Lambda_{\hat{H}S_1} + \Lambda_{\tilde{H}S_1} + \Lambda_{\widetilde{ISI}} + \Lambda_N)^{-1})\Lambda_{\hat{H}S_1,S_1} && \text{(D.16)}
\end{aligned}$$

$$\Lambda_E^{-1} = \Lambda_{S_1}^{-1} + \hat{H}^T(\Lambda_{\tilde{H}S_1} + \Lambda_{\widetilde{ISI}} + \Lambda_N)^{-1}\hat{H} \tag{D.17}$$

$$\begin{aligned}
I(S_1, Y) &\geq \frac{1}{2}\log(|\Lambda_{S_1}||\Lambda_E^{-1}|) && \text{(D.18)}\\
&= \frac{1}{2}\log(|\Lambda_{S_1}||\Lambda_{S_1}^{-1} + \hat{H}^T(\Lambda_{\tilde{H}S_1} + \Lambda_{\widetilde{ISI}} + \Lambda_N)^{-1}\hat{H}|) && \text{(D.19)}\\
&= \frac{1}{2}\log(|I_4 + \hat{H}^T(\Lambda_{\tilde{H}S_1} + \Lambda_{\widetilde{ISI}} + \Lambda_N)^{-1}\hat{H}\Lambda_{S_1}|) && \text{(D.20)}\\
&= \frac{1}{2}\log(|I_4 + (\Lambda_{\tilde{H}S_1} + \Lambda_{\widetilde{ISI}} + \Lambda_N)^{-1}\hat{H}\Lambda_{S1}\hat{H}^T|) && \text{(D.21)}\\
&= \frac{1}{2}\log((\frac{\sigma_s^2(h_{1,R}^2 + h_{2,R}^2 + h_{1,I}^2 + h_{2,I}^2)}{\sigma_n^2 + 4\sigma_{\tilde{h}}^2\sigma_s^2} + 1)^2) && \text{(D.22)}\\
&= \log(\frac{\sigma_s^2(h_{1,R}^2 + h_{2,R}^2 + h_{1,I}^2 + h_{2,I}^2)}{\sigma_n^2 + 4\sigma_{\tilde{h}}^2\sigma_s^2} + 1) && \text{(D.23)}
\end{aligned}$$

Appendix E
Derivation of DS-CDMA Region

Our DS-CDMA system is the most complicated of the four schemes because it experiences both ISI and multi-user interference. Thus, we will need to deal with more terms than in the previous cases. In order to make sense of it all, we urge the reader to refer to Figures 3.9 and 3.10.

We start by defining the terms that shape our desired signal. Note that since we have both ISI and multi-user interference, all of our signal terms now have two indices: user index and symbol index.

$$S1,1 = \begin{pmatrix} s_{1,1,R} \\ s_{1,1,I} \end{pmatrix} \tag{E.1}$$

$$C_1 = \begin{pmatrix} c_{1,1,R} & -c_{1,1,I} \\ c_{1,2,R} & -c_{1,2,I} \\ c_{1,1,I} & c_{1,1,R} \\ c_{1,2,I} & c_{1,2,R} \end{pmatrix} \tag{E.2}$$

$$H = \begin{pmatrix} h_{1,R} & 0 & -h_{1,I} & 0 \\ h_{2,R} & h_{1,R} & -h_{2,I} & -h_{1,I} \\ 0 & h_{2,R} & 0 & -h_{2,I} \\ h_{1,I} & 0 & h_{1,R} & 0 \\ h_{2,I} & h_{1,I} & h_{2,R} & h_{1,R} \\ 0 & h_{2,I} & 0 & h_{2,R} \end{pmatrix} \tag{E.3}$$

Next we define the terms that shape the ISI terms.

$$S_1^{ISI} = \begin{pmatrix} s_{1,0,R} \\ s_{1,2,R} \\ s_{1,0,I} \\ s_{1,2,I} \end{pmatrix} \tag{E.4}$$

$$C_1^{ISI} = \begin{pmatrix} c_{1,2,R} & 0 & -c_{1,2,I} & 0 \\ 0 & 0 & 0 & 0 \\ 0 & c_{1,1,R} & 0 & -c_{1,1,I} \\ c_{1,2,I} & 0 & c_{1,2,R} & 0 \\ 0 & 0 & 0 & 0 \\ 0 & c_{1,1,I} & 0 & c_{1,1,R} \end{pmatrix} \tag{E.5}$$

$$H^{ISI} = \begin{pmatrix} h_{2,R} & 0 & 0 & -h_{2,I} & 0 & 0 \\ 0 & 0 & 0 & 0 & 0 & 0 \\ 0 & 0 & h_{1,R} & 0 & 0 & -h_{1,I} \\ h_{2,I} & 0 & 0 & h_{2,R} & 0 & 0 \\ 0 & 0 & 0 & 0 & 0 & 0 \\ 0 & 0 & h_{1,I} & 0 & 0 & h_{1,R} \end{pmatrix} \tag{E.6}$$

Because multipath increases the duration of the signal (the "interval of interest"), we use a special despreading matrix that is delay-matched to the channel output.

$$C_{1,D} = \begin{pmatrix} c_{1,1,R} & c_{1,2,R} & 0 & c_{1,1,I} & c_{1,2,I} & 0 \\ 0 & c_{1,1,R} & c_{1,2,R} & 0 & c_{1,1,I} & c_{1,2,I} \\ -c_{1,1,I} & -c_{1,2,I} & 0 & c_{1,1,R} & c_{1,2,R} & 0 \\ 0 & -c_{1,1,I} & -c_{1,2,I} & 0 & c_{1,1,R} & c_{1,2,R} \end{pmatrix} \tag{E.7}$$

Before we begin defining covariance matrices, we need to define some terms based on spreading code properties of the two users. This will ease our notation later.

$$t_{1,1} = c_{1,2,R}c_{1,1,R} + c_{1,2,I}c_{1,1,I} \tag{E.8}$$

$$t_{1,2} = c_{1,2,R}c_{1,1,I} - c_{1,2,I}c_{1,1,R} \tag{E.9}$$

$$
\begin{aligned}
t_{2,1} &= c_{1,1,R}c_{2,1,R} + c_{1,1,I}c_{2,1,I} && \text{(E.10)}\\
t_{2,2} &= c_{1,1,R}c_{2,2,R} + c_{1,2,I}c_{2,2,I} && \text{(E.11)}\\
t_{2,3} &= c_{1,1,I}c_{2,1,R} - c_{1,1,R}c_{2,1,I} && \text{(E.12)}\\
t_{2,4} &= c_{1,2,I}c_{2,2,R} - c_{1,2,R}c_{2,2,I} && \text{(E.13)}\\
t_{2,5} &= c_{1,1,R}c_{2,2,R} + c_{1,1,I}c_{2,2,I} && \text{(E.14)}\\
t_{2,6} &= c_{1,1,I}c_{2,2,R} - c_{1,1,R}c_{2,2,I} && \text{(E.15)}\\
t_{2,7} &= c_{1,2,R}c_{2,1,R} + c_{1,2,I}c_{2,1,I} && \text{(E.16)}\\
t_{2,8} &= c_{1,2,I}c_{2,1,R} - c_{1,2,R}c_{2,1,I} && \text{(E.17)}
\end{aligned}
$$

Now we begin with the simplest covariance matrices that we will need.

$$
\begin{aligned}
\Lambda S_{1,1} &= \sigma_{s_1}^2 I_2 && \text{(E.18)}\\
\Lambda N &= \sigma_n^2 I_4 && \text{(E.19)}
\end{aligned}
$$

Next we calculate the covariance of the unresolvable signal of the first user (which will function as self-interference).

$$
\Lambda_{C_1\tilde{H}C_1S_1} = E[(C_{1,D}\tilde{H}C_1S_1)(C_{1,D}\tilde{H}C_1S_1)^T] \tag{E.20}
$$

$$= \begin{pmatrix} \frac{5}{2} & 4t_{1,1} & 0 & -4t_{1,2} \\ 4t_{1,1} & \frac{5}{2} & 4t_{1,2} & 0 \\ 0 & 4t_{1,2} & \frac{5}{2} & 4t_{1,1} \\ -4t_{1,2} & 0 & 4t_{1,1} & \frac{5}{2} \end{pmatrix} \sigma_{s_1}^2 \sigma_{\tilde{h}}^2 \tag{E.21}$$

Then comes the covariance of the same-user ISI that we are unable to cancel. Notice that the elements of the ISI matrix are orthogonal to each other in time, so we have a diagonal matrix.

$$\Lambda_{C_{1,D}\tilde{H}^{ISI}C_1^{ISI}S_1^{ISI}} = E[(C_{1,D}\tilde{H}^{ISI}C_1^{ISI}S_1^{ISI})(C_{1,D}\tilde{H}^{ISI}C_1^{ISI}S_1^{ISI})^T] \tag{E.22}$$

$$= (2\sigma_{s_1}^2\sigma_{\tilde{h}}^2 t_{1,1}^2 + 2\sigma_{s_1}^2\sigma_{\tilde{h}}^2 t_{1,2}^2) I_4 \tag{E.23}$$

$$= \frac{1}{2}\sigma_{s_1}^2\sigma_{\tilde{h}}^2 I_4 \tag{E.24}$$

Next, we address the covariance matrices of the multi-user interference. We start with the second user's signal of interest. That is, the component of the multi-user interference that is dependent on the signal at symbol index 1.

$$\begin{aligned} \Lambda C_{1,D}\tilde{H}C_2S_2 &= E[(C_{1,D}\tilde{H}C_2S_2)(C_{1,D}\tilde{H}C_2S_2)^T] \\ &= \begin{pmatrix} A & B \\ B^T & A \end{pmatrix} \sigma_{s_2}^2\sigma_{\tilde{h}}^2 \end{aligned}$$

We have divided our covariance matrix into the following components.

$$A = \begin{pmatrix} \left(\frac{3}{2} + 4t_{2,1}t_{2,2} + 4t_{2,3}t_{2,4}\right) & 2\begin{pmatrix} t_{2,5}t_{2,2} + t_{2,5}t_{2,1} + t_{2,6}t_{2,3} \\ +t_{2,6}t_{2,4} + t_{2,3}t_{2,8} + t_{2,4}t_{2,8} \end{pmatrix} \\ 2\begin{pmatrix} t_{2,5}t_{2,2} + t_{2,5}t_{2,1} + t_{2,6}t_{2,3} \\ +t_{2,6}t_{2,4} + t_{2,3}t_{2,8} + t_{2,4}t_{2,8} \end{pmatrix} & \left(\frac{3}{2} + 4t_{2,1}t_{2,2} + 4t_{2,3}t_{2,4}\right) \end{pmatrix} \tag{E.25}$$

$$B = \begin{pmatrix} 0 & 2\begin{pmatrix} -t_{2,1}t_{2,6} + t_{2,2}t_{2,6} + t_{2,3}t_{2,5} \\ +t_{2,4}t_{2,5} + t_{2,8}t_{2,1} + t_{2,8}t_{2,2}) \end{pmatrix} \\ -2\begin{pmatrix} -t_{2,1}t_{2,6} + t_{2,2}t_{2,6} + t_{2,3}t_{2,5} \\ +t_{2,4}t_{2,5} + t_{2,8}t_{2,1} + t_{2,8}t_{2,2} \end{pmatrix} & 0 \end{pmatrix} \tag{E.26}$$

Finally, we add the covariance of the second user's adjacent symbols, the user 2 ISI.

$$\Lambda C_{1,D}\tilde{H}^{ISI}C_2^{ISI}S_2^{ISI} = E[(C_{1,D}\tilde{H}^{ISI}C_2^{ISI}S_2^{ISI})(C_{1,D}\tilde{H}^{ISI}C_2^{ISI}S_2^{ISI})^T] \tag{E.27}$$

$$= \begin{pmatrix} 2(t_{2,5}^2 + t_{2,6}^2) & 0 & 0 & 0 \\ 0 & 2(t_{2,7}^2 + t_{2,8}^2) & 0 & 0 \\ 0 & 0 & 2(t_{2,5}^2 + t_{2,6}^2) & 0 \\ 0 & 0 & 0 & 2(t_{2,7}^2 + t_{2,8}^2) \end{pmatrix} \sigma_{s_2}^2\sigma_{\tilde{h}}^2 \tag{E.28}$$

$$= \frac{1}{2}\sigma_{s_2}^2\sigma_{\tilde{h}}^2 I_4 \tag{E.29}$$

$$I(S_1,Y) \geq \frac{1}{2}\log(\left| \begin{pmatrix} \Lambda N + \Lambda_{C_1\tilde{H}C_1S_1} + \Lambda_{C_1\tilde{H}C_2S_2} \\ +\Lambda C_1\tilde{H}^{ISI}C_1^{ISI}S_1^{ISI} + \Lambda C_1\tilde{H}^{ISI}C_2^{ISI}S_2^{ISI} \end{pmatrix}^{-1} \hat{H}\Lambda_{S_1}\hat{H}^T + I \right|) \tag{E.30}$$

References

1. C.E. Shannon, "A Mathematical Theory of Communication," Bell Sys. Technical Journal, vol. 27, pp. 379-423, 623-656, 1948.

2. S. Verdu, S. Shamai (Shitz), "Spectral Efficiency of CDMA with Random Spreading," IEEE Transactions on Information Theory, vol. 45, no. 2, pp. 622-640, March 1999

3. S. Shamai (Shitz), S. Verdu, "The Impact of Frequency-Flat Fading on the Spectral Efficiency of CDMA," IEEE Transactions on Information Theory, vol. 47, no. 4, pp. 1302-1327, May 2001

4. G. Stuber, *Principles of Mobile Communication.* Kluwer Academic Publishers, Norwell, Mass.: 1996.

5. B.D.O. Anderson, J.B. Moore, *Optimal Filtering.* Prentice Hall, Englewood Cliffs, NJ: 1979.

6. H. Stark, J.W. Woods, *Probability and Random Processes with Applications to Signal Processing.* Prentice Hall, Upper Saddle River, NJ: 2002.

7. J.G. Proakis, M. Salehi, *Communication Systems Engineering.* Prentice Hall, Upper Saddle River, NJ: 1994.

8. T.M. Cover, J.A. Thomas, *Elements of Information Theory.* Wiley, New York: 1991.

9. J.G. Proakis, *Digital Communications.* McGraw Hill, New York: 2001.

10. S. Verdu, *Multiuser Detection.* Cambridge University Press, Cambridge, UK: 1998.

11. T.S. Rappaport, *Wireless Communications.* Prentice Hall, Upper Saddle River, NJ: 1996.

12. G. Caire, D. Tuninetti, S. Verdu, "Suboptimality of TDMA in the Low Power Regime," Submitted to IEEE Transactions on Information Theory, Sept. 2002.

13. I.E. Telatar, D.N.C. Tse, "Capacity and Mutual Information of Wideband Multipath Fading Channels," IEEE Transactions on Information Theory, vol. 46, no. 4, pp. 1384-1400, Jul. 2000.

14. D.N.C. Tse, S.V. Hanly, "Multiaccess Fading Channels–Part I: Polymatroid Structure, Optimal Resource Allocation and Throughput Capacities," IEEE Transactions on Information Theory, vol. 44, no. 7, pp. 2796-2815, Nov. 1998.

15. S.V. Hanly and D.N.C. Tse, "Multiaccess Fading Channels–Part II: Delay-Limited Capacities," IEEE Transactions on Information Theory, vol. 44, no. 7, Nov. 1998.

16. A.J. Goldsmith, "The Capacity of Down link Fading Channels with Variable Rate and Power," IEEE Transactions on Vehicular Technology, vol. 46, no. 3, pp. 569-580, Aug. 1997.

17. A.M. Viterbi, A.J. Viterbi, "Erlang Capacity of a Power Controlled CDMA System," IEEE Journal on Selected Areas in Communications, vol. 11, no. 6, pp. 892-900, Aug. 1993.

18. M. Medard, "The Effect upon Channel Capacity in Wireless Communications of Perfect and Imperfect Knowledge of the Channel," IEEE Transactions on Information Theory, vol. 46, no. 3, pp. 933-946, May 2000.

19. B. Hassibi, B.M. Hochwald, "How Much Training is Needed in Multiple-Antenna Wireless Links?" IEEE Transactions on Information Theory, vol. 49, no. 4, pp. 951-963, April 2003.

20. S. Bhashyam, A. Sabharwal, B. Aazhang, "Feedback Gain in Multiple Antenna Systems," IEEE Transactions on Communications, vol. 50, no. 5, pp. 785-798, May 2002.

21. M. Medard, "Channel Uncertainty in Communications," IEEE Information Theory Society Newsletter, vol. 53, no. 2, June 2003.

22. J. Andrews and T. Meng, "Optimum Power Control for Successive Interference Cancellation with Imperfect Channel Estimation," IEEE Transactions on Wireless Communications, vol. 2, no. 2, pp. 375-383, March 2003.

23. J. Andrews and T. Meng, "Multiple Access Interference Cancellation in Fading Multipath Channels: Progress and Limitations," Vehicular Technology Conference, VTC 2001 Spring. IEEE VTS 53rd, vol. 1, pp. 614-618, May 2001.

24. L. Li and A.J. Goldsmith, "Capacity and Optimal Resource Allocation for Fading Broadcast Channels–Part I: Ergodic Capacity," IEEE Transactions on Information Theory, vol. 47, no. 3, pp. 1083-1102, March 2001.

25. L. Li and A.J. Goldsmith, "Capacity and Optimal Resource Allocation for Fading Broadcast Channels–Part II: Outage Capacity," IEEE Transactions on Information Theory, vol. 47, no. 3, pp. 1103-1127, March 2001.

26. P.P. Bergmans and T.M. Cover, "Cooperative Broadcasting," IEEE Transactions on Information Theory, vol. 20, no. 3, pp. 317-324, May 1974.

27. T.M. Cover, "Broadcast Channels," IEEE Transactions on Information Theory, vol. 18, no. 1, pp. 2-14, Jan. 1972.

28. D. Scott, "On Optimal and Data-Based Histograms," Biometrika, vol. 66, pp. 605-610, 1979.